REPORT DOCUMENTATION PAGE

Form Approved
OMB No. 0704-0188

PLEASE DO NOT RETURN YOUR FORM TO THE ABOVE ADDRESS.

1. REPORT DATE *(DD-MM-YYYY)*	2. REPORT TYPE	3. DATES COVERED *(From - To)*
2004	Journal Article Reprint	2004

4. TITLE AND SUBTITLE

Fate of Ammonia in the Atmosphere -- a Review for Applicability to Hazardous Releases

5a. CONTRACT NUMBER

F08637-99-C-6004

5b. GRANT NUMBER

5c. PROGRAM ELEMENT NUMBER

62102F

6. AUTHOR(S)

Jean J. Renard, Sheryl E. Calidonna and Michael V. Henley

5d. PROJECT NUMBER

5e. TASK NUMBER

5f. WORK UNIT NUMBER

4915E20D

7. PERFORMING ORGANIZATION NAME(S) AND ADDRESS(ES)

Air Force Research Laboratory
Airbase Technologies Division
139 Barnes Drive, Suite 2
Tyndall AFB FL 32403-5323

8. PERFORMING ORGANIZATION REPORT NUMBER

AFRL-ML-TY-TP-2003-4541

9. SPONSORING/MONITORING AGENCY NAME(S) AND ADDRESS(ES)

10. SPONSOR/MONITOR'S ACRONYM(S)

11. SPONSOR/MONITOR'S REPORT NUMBER(S)

12. DISTRIBUTION/AVAILABILITY STATEMENT

Distribution Statement "A". Distribution Unlimited

13. SUPPLEMENTARY NOTES

Published in the Journal of Hazardous Materials B108 (2004) pp 29-60

14. ABSTRACT

The physical and chemical mechanisms responsible for the removal of ammonia from the atmosphere have been reviewed. Capture by atmospheric moisture (clouds, rain, fog), surface waters (rivers, lakes, seas), and deposition on vegetation and soil constitute the main pathways for ammonia removal from the troposphere. Ammonia catalyzes the atmospheric oxidation of sulfur dioxide to sulfur trioxide and reacts rapidly with acidic components of the atmosphere (sulfuric, nitric, and hydrochloric acids). The ammonium salts formed are the main components of smog aerosols and thus affect the opacity of the atmosphere and the earth radiation budget. Slow oxidation of ammonia in the atmosphere plays only a minor role in its removal. The data obtained for ammonia reactions under normal atmospheric conditions are generally applicable to model chemical reactions occurring during massive release of ammonia in the atmosphere, provided the impact of high ammonia concentration on the mass transfer processes that control some of these reactions, are taken into account.

15. SUBJECT TERMS

16. SECURITY CLASSIFICATION OF:			17. LIMITATION OF ABSTRACT	18. NUMBER OF PAGES	19a. NAME OF RESPONSIBLE PERSON
a. REPORT	b. ABSTRACT	c. THIS PAGE			Lt Lindsey Sorensen
U	U	U	SAR	32	19b. TELEPHONE NUMBER *(Include area code)* 850-283-6050

ELSEVIER

Journal of Hazardous Materials B108 (2004) 29–60

Journal of Hazardous Materials

www.elsevier.com/locate/jhazmat

Review

Fate of ammonia in the atmosphere—a review for applicability to hazardous releases

Jean J. Renard [a], Sheryl E. Calidonna [a], Michael V. Henley [b,*]

[a] *Applied Research Associates, Inc., Airbase Technologies Division, 139 Barnes Drive, Suite 2, Tyndall AFB, FL 32403-5323, USA*

[b] *Air Force Research Laboratory, Airbase Technologies Division, 139 Barnes Drive, Suite 2, Tyndall AFB, FL 32403-5323, USA*

Received 28 July 2003; received in revised form 22 January 2004; accepted 22 January 2004

Abstract

The physical and chemical mechanisms responsible for the removal of ammonia from the atmosphere have been reviewed. Capture by atmospheric moisture (clouds, rain, fog), surface water (rivers, lakes, seas), and deposition on vegetation and soil constitute the main pathways for ammonia removal from the troposphere. Ammonia catalyzes the atmospheric oxidation of sulfur dioxide to sulfur trioxide and reacts rapidly with acidic components of the atmosphere (sulfuric, nitric, and hydrochloric acids). The ammonium salts formed are the main components of smog aerosols and thus affect the opacity of the atmosphere and the earth radiation budget. Slow oxidation of ammonia in the atmosphere plays only a minor role in its removal. The data obtained for ammonia reactions under normal atmospheric conditions are generally applicable to model chemical reactions occurring during massive release of ammonia in the atmosphere, provided the impact of high ammonia concentration on the mass transfer processes that control some of these reactions, are taken into account.

Keywords: Ammonia; Atmospheric chemistry; Plume dispersion; Modeling; Catastrophic release

1. Introduction

The long-standing concern for public safety in cases of accidental releases of toxic materials from chemical plants has gained additional momentum from recent fear of terrorist attacks on chemical plants or the chemical transportation system. In cases of accidental or malicious massive release of hazardous chemicals in the environment, it is essential that first responders have an accurate forecast of the spatial and temporal distribution of released toxic chemicals to decide on population evacuation needs and to plan remedial measures.

A number of mathematical models exist that adequately describe the dispersion of a plume of chemicals based on prevailing meteorological conditions, terrain profiles, and physical properties of released chemicals. Recent advances in computer technology allow these models to be run quickly and effectively from laptop computers, thus making them readily available to civil authorities directing the response to chemical incidents. However, these models generally lack an accurate description of chemical transformations that the released chemicals will undergo in the atmosphere. As a starting point in our effort to correct this deficiency, we have prepared this review of the present knowledge of atmospheric reactions of ammonia, placing particular emphasis on kinetics of the reactions involved and in identifying missing elements for a comprehensive incorporation of chemical atmospheric behavior of ammonia as part of a realistic plume dispersion model. The selection of ammonia stems from its economic importance and widespread distribution throughout the country for industrial and agricultural use. Following this critical review of the significant body of knowledge on the atmospheric chemistry of ammonia, recommendations will be presented for additional investigations required to generate the data needed for an adequate description of the chemical be-

* Corresponding author.
E-mail address: mike.henley@tyndall.af.mil (M.V. Henley).

0304-3894/$ – see front matter © 2004 Elsevier B.V. All rights reserved.
doi:10.1016/j.jhazmat.2004.01.015

havior of high concentration plumes of ammonia in the atmosphere.

2. Aqueous chemistry of ammonia

2.1. Dissociation of ammonia in aqueous solutions

In aqueous solutions, NH_3 is partially hydrolyzed to ammonium hydroxide according to Eq. (1):

$$(NH_3)aq + H_2O \leftrightarrow NH_4^+ + OH^- \quad (1)$$

with an equilibrium constant $K_b = 1.774 \times 10^{-5}$ at 25 °C (298 K) [1]. Eq. (2) represents the best fit of the values of K_b determined by Bates and Pinching over the 0–40 °C temperature range [2].

$$\ln K_b = 16.9732 - \frac{4411.025}{T} - 0.0440T \quad (2)$$

where the temperature, T, is in Kelvin (T (K) = 273.15 + °C).The pH of the aqueous solution strongly influences the reactions establishing equilibrium 1. In solutions of ammonia in water or in aqueous solutions at neutral and alkaline pH, the following rate constants have been measured using electric field pulse/conductimetric techniques [3,4]:

$$(NH_3)aq + H_2O \rightarrow NH_4^+ + OH^-, \quad k_{295\,K} = 5 \times 10^5\ s^{-1} \quad (3)$$

$$NH_4^+ + OH^- \rightarrow (NH_3)aq + H_2O, \quad k_{295\,K} = 3 \times 10^{10}\ M^{-1}\ s^{-1} \quad (4)$$

In the acid pH range, similarly fast reaction rates were determined using nuclear magnetic resonance techniques [5].

$$(NH_3)aq + H^+ \rightarrow NH_4^+, \quad k_{295\,K} = 4.3 \times 10^{10}\ M^{-1}\ s^{-1} \quad (5)$$

$$NH_4^+ \rightarrow (NH_3)aq + H^+, \quad k_{295\,K} = 24.6\ s^{-1} \quad (6)$$

2.2. Solubility of ammonia in aqueous solutions

2.2.1. Solubility in pure water

Equilibrium partial pressure data for NH_3 above pure aqueous solutions are available over a wide range of temperature and concentrations. A complete review and critical evaluation of the data was conducted in 1989 and published by Clegg and Brimblecombe [2].

$$(NH_3)g \leftrightarrow (NH_3)aq \quad (7)$$

$$(NH_3)aq + H_2O \leftrightarrow NH_4^+ + OH^- \quad (1)$$

The solubility of a weak electrolyte such as NH_3 can be described in two stages; as dissolution followed by base dissociation, yielding the following equations for thermodynamic Henry's law constant K_H (mol kg^{-1} atm^{-1}), and base dissociation constant K_B (mol kg^{-1}):

$$K_H = \frac{\gamma_{NH_3} m_{NH_3}}{p_{NH_3}} \quad (\text{from Eq. (7)}) \quad (8)$$

$$K_B = \frac{\gamma_{NH_4} m_{NH_4} \gamma_{OH} m_H}{\gamma_{NH} m_{NH_3} a_w} \quad (\text{from Eq. (1)}) \quad (9)$$

where m denotes molality (mol kg^{-1}), p the partial pressure (atm), γ denotes the activity coefficient, and a_w the activity of water.

To determine Henry's law constant experimentally, two quantities are measurable: the partial pressure of NH_3, p_{NH_3}, over the solution, and the total concentration of ammonium species in solution: $NH_3 + NH_4^+ = N_{tot}$. To compute K_H, the activity of $(NH_3)aq$ must be estimated from the measured N_{tot} and K_B, applying appropriate approximations for the activity coefficients of the species involved, depending on the characteristics of the aqueous solution used. For example, if the solution is dilute enough, the activity coefficients can be assumed to be equal to 1. Many of the differences for the value of K_H found in the literature can be explained by the difference in the choices made in the estimation of the activity coefficients. The most recent determinations of K_H are summarized in Table 1.

The values of K_H reported by Hales and Drewes [6] are clearly higher than those of other investigators, a situation

Table 1
Determination of Henry's law constant

Reference	$\ln K_H = f(T)$ (K_H: kg atm mol^{-1})	K_H (kg atm mol^{-1}), 273.15 K (0 °C)	K_H (kg atm mol^{-1}), 283.15 K (10 °C)	K_H (kg atm mol^{-1}), 298.15 K (25 °C)
Hales and Drewes [6]		231.92	144.10	75.45
Edwards et al. [7]	160.559 − (8.621.06/T) −(25.6767 ln T) + 0.035388T	217.72	126.19	60.80
Dasgupta and Dong [8]	−9.70 + (4092/T)	196.52	115.78	55.96
Clegg and Brimblecombe [2]	−8.09694 + (3917.507/T) − (0.00314T)	218.62	127.66	60.72
Shi et al. [9]	−3.221 + (1396/T)	77.58	51.19	28.92
Thermodynamic value calculated from NBS data [10]	− 9.94 + (4166/T)	202.58	118.28	56.42
Thermodynamic value calculated from Wagman data [11]				57.64

resulting most likely from poor management of temperature changes and control in the experimental procedures, as discussed by Dasgupta and Dong [8]. At the other extreme, Shi et al. [9] report values that are much lower than other researchers. Whereas, other investigators ensure the systems are at equilibrium before measuring ammonia pressure above its aqueous solution, Shi et al. used a droplet train flow reactor in which, from their own admission ([9], p. 8816) "under the conditions of the droplet experiments, equilibrium is not attained and the pH near the surface is time dependent". Their values for K_H are derived from the model of kinetics of the process and from the kinetics data that show significant uncertainty, particularly at the high end of their temperature range. Moreover, they used a train of aqueous sodium hydroxide solution (pH 13) droplets to maintain alkaline pH during the experiment. The salting-out effect of sodium hydroxide, reportedly 10%, was taken into account using an unspecified methodology to estimate magnitude. The accuracy of the values for K_H is therefore open to question. In a later note [12], the authors recognized the shortcomings of their analysis and confirmed the reported value for K_H was too low.

With the exception of the two investigations discussed above, the remainder of the investigation report values for K_H are within less than 10% of each other. Dasgupta and Dong [8] used dilute solution ammonia (0.002–0.1 M) in phosphate buffers (pH 6–10). The activity coefficient for the ammonium ion was calculated using the model of Laitinen and Harris [13] that accounts for the effect of the overall ionic strength of the solution and the activity coefficient for (NH_3)aq was set as 1. Edwards et al. [7] re-analyzed the data of Van Krevelen et al. [14] using a thermodynamic approach where the vapor phase coefficient of ammonia over the solution is estimated from the second coefficient of the virial equation of state for pure ammonia. Given the relatively high concentration of ammonia used and the very low value for K_b (1.774×10^{-5} at 25 °C), they neglected ammonia dissociation and used Eq. (10) to estimate the activity coefficient of aqueous ammonia.

$$\ln \gamma_N = 2\beta_{NN} m_N \tag{10}$$

where subscript N is thereafter used to designate NH_3, γ_N is the activity coefficient for undissociated aqueous ammonia, β_{NN} the two-body interaction coefficient for aqueous ammonia, and m_N is the molality of ammonia in water.

Equating the chemical potentials of ammonia in the aqueous solution and in the gas phase and neglecting the vapor pressure of water as much smaller than the total system pressure, leads to Eq. (11)

$$\ln\left(\frac{\Phi_N P}{m_N}\right) - \left(\frac{v_N P}{RT}\right) = \ln K_H + 2\beta_{NN} m_N \tag{11}$$

where Φ_N is the fugacity coefficient for gaseous ammonia: $\exp(B_N P/RT)$, B_N second coefficient of virial equation of state for pure ammonia, and v_N is the partial molar volume of ammonia (30.0 at 25 °C).

The left side of Eq. (11) is computed from experimental values and plotted against m_N. The intercept gives the value of $\ln K_H$ and the slope the value of $2\beta_{NN}$.

Clegg and Brimblecombe [2] re-analyzed the data of Chen et al. [15], neglecting the dissociation of the base in the relatively concentrated ammonia solutions in pure water used by Chen et al. [15], considering the low value of K_b (1.774×10^{-5} at 25 °C).

The values of K_H reported by these three last investigations are in fairly close agreement with those calculated using available free energy and enthalpy data (NBS data). Therefore, within a 10% maximum accuracy range, the results of these investigations are in good agreement and consistent with those of thermodynamic calculations.

Considering that in the intended application, high concentration of ammonia, will be involved together with water with low dissolved salt content (rain drops), we recommend using the relationship developed by Clegg and Brimblecombe [2] because it was derived from data obtained at high concentrations of ammonia in pure water.

2.2.2. *Solubility in multi-component aqueous solutions*

When ammonia is released in the environment, it will interact with water sources containing significant quantities of dissolved chemicals e.g., seawater or condensation droplets with dissolved atmospheric pollutants. The solubility of ammonia will be influenced by the presence of the dissolved chemicals. Two main approaches have been used to compute the solubility of ammonia in multi-component aqueous solutions.

As discussed earlier, Edwards et al. [7] used a thermodynamic approach to analyze the equilibrium of ammonia between the aqueous solution and the gas phase and derive a general formulation for the activity coefficient of ammonia in aqueous solution represented by Eq. (12):

$$\ln \gamma_I = \left(\frac{\alpha z^+ z^- I^{1/2}}{1 + I^{1/2}}\right) + 2\sum \beta_{ij} m_j \tag{12}$$

where α is the Debye–Huckel parameter (0.391 at 25 °C), z^+z^- the charges of the cation and anion of compound I, I the ionic strength of the solution ($\Sigma m_i z_i$), β_{ij} the two-body interaction coefficient of component i with component j, and m_j is the molality of component j.

This expression represents the deviation from non-ideality due to specific interaction between the components in the solution:

- The first term represents the contribution of electrostatic interaction between charge ions, based on Debye–Huckel's theory of very dilute electrolyte solutions.
- The second term is a summation of all the short-range two-body interactions between the components in the solution:
  - molecule-to-molecule Vander Waals interactions;
  - molecule-ionic species interactions (salting-out effect);
  - ions-to-ions interactions other than electrostatic.

Table 2
Molecule–molecule interactions for single solute

Solute, I	β_{ii} (kg water mol^{-1})
NH_3	0.017
CO_2	0.010
SO_2	−0.277
H_2S	0.005

Table 3
Ion–ion specific interaction parameters

Ion, I	β_{ii} (kg water mol^{-1})
NH_4^+	−0.12
HCO_3^-	0.25
CO_3^-	−0.12
HSO_3^-	0.24
SO_3^-	−0.05
NH_2COO^-	0.33
H^+	0.10
OH^-	0.15

These interactions coefficient, β_{ij} are determined empirically, as illustrated in the preceding section for the case of ammonia in pure water solution. In this case, dissociation of ammonia was neglected, thus zeroing the electrostatic interaction term, and ammonia was the only species in solution, thus $\beta_{ij} = \beta_{NN}$, and Eq. (12) reduces to Eq. (10). This approach was used to determine empirically the various interaction coefficients reported in Tables 2–4.

The values for the appropriate parameters are inserted in Eq. (12) to obtain the value for $\ln \gamma_N$ that, together with Eq. (13), is used to characterize the distribution of NH_3 between the gas phase and the aqueous solution.

$$y_N \Phi_N P = K_H \gamma_N m_N \tag{13}$$

where y_N is the molar fraction of NH_3 in the gas phase.

Clegg and Brimblecombe [2] used a like approach based on a more sophisticated model of Pitzer [16] to calculate activity coefficients in a mixed electrolyte solution using a virial expansion of terms of concentration. The functions involved are quite complex, particularly for ionic species. For neutral species like undissociated ammonia, the activity coefficient is given by Eq. (14):

$$\ln \gamma_N = 2\sum_c \beta_{N_c} m_c + 2\sum_a \beta_{N_a} m_a + 2\sum_n \beta_{N_n} m_n + 3\sum_i \sum_j \mu_{N_{ij}} m_j m_i \tag{14}$$

Table 4
Molecule–ion specific interaction parameters

Molecule–ion, $ij = nj$	β_{Nj} (kg water mol^{-1})
NH_3–HCO_3^-	−0.031
NH_3–CO_3^-	0.068
NH_3–HSO_3^-	−0.038
NH_3–SO_3^-	0.044
NH_3–NH_2COO^-	−0.028
NH_3–H^+	0.015
NH_3–OH^-	0.021

Table 5
Interaction parameters for NH_3 at 25 °C

Species, I	β_{Ni}	μ_{NNi}
NH_3	0.01472	
Mg^{2+}	−0.21	
Ca^{2+}	−0.081	
Li^+	−0.038	
Na^+	0.0175	−0.000311
K^+	0.0454	−0.000321
NH_4^+	0	−0.00075
Cl^-	0	
OH^-	0.103	
NO_3^-	−0.01	−0.000437
SO_3^{2-}	0.158	
SO_4^{2-}	0.140	
CO_3^{2-}	0.180	0.000625
NO_2^-	−0.003	

where β_{N_c} is the ammonia-cation interaction parameter, the β_{N_a} ammonia-anion interaction parameter, β_{N_n} the ammonia-neutral molecule interaction parameter, $\mu_{N_{ij}}$ the ammonia-species i–species j (three-bodies interaction parameter), and m_i the molality of species i.

Clegg and Brimblecombe [2] conducted an extensive review and analysis of the literature on the solubility of ammonia in a variety of electrolyte solutions and determined and compiled values for various interaction parameters. Table 5 summarizes their results for the species of interest to this project.

It should be noted that the values of β_{NN} found in these two investigations are in good agreement: 0.01472 (Table 5) and 0.017 (Table 2). In general, for solutions that are not too concentrated ($m_i < 1.5$ mol kg^{-1}), the three bodies interaction can be neglected.

Although more complex, Pitzer's approach has been found repeatedly to describe accurately the behavior of complex electrolyte solutions such as seawater, brine, and industrial solutions. Its use is recommended to estimate the solubility of ammonia in concentrated salt solutions.

2.3. Uptake of gaseous ammonia by water surfaces—mass accommodation coefficient

2.3.1. Modeling gas–liquid interactions

In a recent paper, Shi et al. [9] gave an excellent phenomenological description of the interactions between gas and liquid with specific application to the ammonia–water interaction. The process can essentially be described as a sequence of the following steps:

- The gas molecule is transported to the liquid surface, usually by gas-phase diffusion.
- The gas molecule strikes the surface of the liquid and is thermally accommodated as an adsorbed surface species.
- Depending on chemical affinity of the gas for the liquid and on the conditions at the surface of the liquid, the following additional steps can occur:

- the adsorbed molecule can desorb from the surface and return to the gas phase;
- the adsorbed molecule can become dissolved in the liquid and migrate into the bulk of the liquid by liquid-phase diffusion;
- the adsorbed molecule can undergo reversible reaction with the liquid, such as ionization, or irreversible reaction with the solvent or dissolved species in the solvent.

The overall process can be modeled using an electrical circuit analogue where each step is analogous to an electrical resistance. The measured uptake of ammonia, γ_{meas}, is inversely proportional to the sum of the resistance representing each elementary step in the process. To develop a mathematical framework for the model, the following parameters are defined:

- The gas molecule strikes the surface of the liquid and is thermally accommodated.
- $1/\Gamma_{diff}$ represents the resistance to gas-phase diffusive transfer. For droplets, the value is estimated using the Fuchs–Sutugin [17] formulation:

$$\frac{1}{\Gamma_{diff}} = \frac{0.75 + 0.283\mathrm{Kn}}{\mathrm{Kn}(1 + \mathrm{Kn})} \quad (15)$$

where Kn is the Knudsen factor defined as $6D_g/cd_f$, D_g the gas-phase diffusion coefficient of ammonia, d_f the effective diameter of the droplet, and c the mean thermal velocity of ammonia in the gas phase

The mass accommodation coefficient, α, represents the probability that a molecule striking the surface of the liquid enters into the bulk of the liquid phase. In the absence of reaction at the interface, the fraction of molecules entering the bulk of the liquid is equal to the fraction of the molecules striking the surface (the adsorption coefficient S) minus the fraction of molecules desorbing from the surface. Consideration of the sorption/desorption equilibrium at the interface leads to:

$$\frac{1}{\alpha} = \frac{(1/S) + k_{des}}{Sk_{sol}} \quad (16)$$

where k_{des} is the rate constant for the desorption process, k_{sol} the rate constant for the passage in solution of the adsorbed molecule, and α is the mass accommodation coefficient, is thus a measure of the ratio of the solution to desorption rate constants.

- Chemical reactions at the interface open a new channel for the removal of the adsorbed gas-phase molecules, distinct from the mass accommodation coefficient, α. These reactions are accounted for by placing an additional resistance, $1/\Gamma_s$, in parallel. The surface uptake coefficient, Γ_s, is proportional to the ratios of the rate constant of the reactions occurring at the interface over the rate constant of the desorption process.
- Solubility and reactions in the bulk of the liquid are usually the main avenues to deplete the interface from adsorbed molecules and to generate free space at the interface to accept new gas-phase molecules. The corresponding bulk uptake coefficient, Γ_b, takes into account the effect on gas uptake of Henry's law solubility, the chemical reaction rates in the bulk of the liquid, and the diffusion coefficients of the species in the liquid. Mathematical description of these phenomena is usually complex and of limited practical utility for modeling purposes.

The measured uptake of ammonia, γ_{meas}, is thus given by:

$$\frac{1}{\gamma_{meas}} = \frac{1}{\Gamma_{diff}} + \frac{1}{S} + \left(\frac{1}{\Gamma_s + (S\alpha/(S-\alpha))} + \frac{1}{\Gamma_b}\right) \quad (17)$$

By applying semi-empirical relationships such as the Fuchs–Sutugin equation (Eq. (15)) to estimate $1/\Gamma_{diff}$, different pH conditions, and known reaction rate constants for ammonia in water, the contributions of the different elemental processes in Eq. (17) can be separated and inferences made about the nature of the species formed at the interface between water and gaseous ammonia.

2.3.2. Experimental determination of the mass accommodation coefficient α

The first determinations of the mass accommodation coefficient for ammonia were made indirectly by measuring the evaporation rates of ammonium nitrate and of chloride from their aqueous solutions [18–20]. In the mathematical treatment of the experimental data, the mass accommodation coefficient is treated as an adjustable parameter, selected to fit the data. In these experiments, ammonia evaporates from the solution together with HCl or NO_3H and possibly with some undissociated salt. The values of α reported varied between 0.02 and 1.

More recent determinations of α by Ponche et al. [21], Bongartz et al. [22], and Shi et al. [9], used the same common approach of measuring the absorption rate of ammonia diluted in a carrier gas into a liquid jet of mono dispersed droplets. Results of these three investigations are in reasonable agreement when differences in temperature and measurement uncertainties are taken into account, as illustrated in Fig. 1. The mass accommodation coefficient increases as the temperature decreases, from 0.08 at 290 K to 0.35 at 260 K.

2.3.3. Mechanism of ammonia dissolution in water

To account for discrepancies between the Gibbs free energy calculated from the temperature dependence of the accommodation coefficients of a series of alcohols and the Gibbs free energy of solvation calculated from the corresponding thermodynamic changes of enthalpy and entropy, Davidovits and co-workers [23,24] have proposed a new model for the uptake of gas molecules by liquids. The model uses the concept that the interface is a narrow region of a dense gas-like state within which nucleation is constantly occurring. Incoming gas molecules participate in the formation of molecular clusters between solvent and gas molecules.

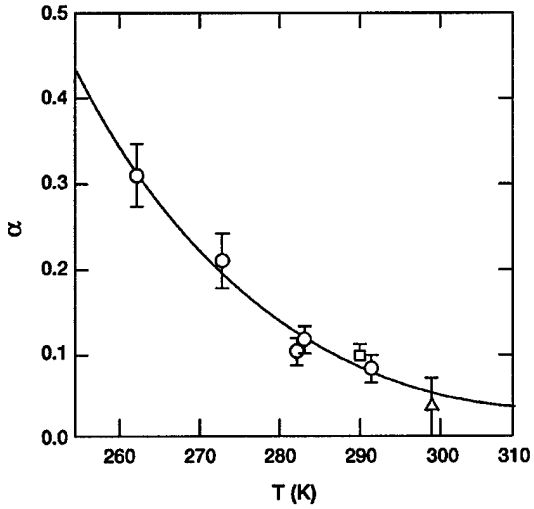

Fig. 1. Temperature dependence of the mass accommodation coefficient of ammonia in water [9].

When the cluster reaches a critical size, it is incorporated in the bulk of the liquid, thereby completing the solvation process and preventing desorption of the now solubilized gas molecules. The change in Gibbs free energy calculated from the temperature dependence of the accommodation coefficient is interpreted to be the activation energy for the formation of the critical size cluster. This model provides a rational explanation for a surprising series of measured changes of enthalpies and entropies for the uptake in water of vapor of alcohols with increasing hydrophobicity.

Donaldson [25] used temperature- and time-dependent surface tension measurements of aqueous ammonia solutions to determine the interfacial binding energies and evaporation rates of ammonia. The values for enthalpy and entropy derived from the equilibrium-tension measurements are consistent with almost fully solvated ammonia in its surface-bound state. Ab initio calculations suggest that ammonia is bound to a small number (two or three) of water molecules at the surface. This complex species would represent the "critical cluster" postulated in Davidovits model that would be easily transferred to the bulk solution. Spectroscopic analysis by Simonelli and Shultz [26] indicates that ammonia is hydrogen bonded to water at the interface, but that ammonia is oriented so that the nitrogen electron pair is bonded to the water's OH group exposed at the liquid surface.

In a subsequent publication, McDuffie [27] analyzed surface tension and vapor–liquid equilibrium data over the complete range of ammonia–water molecular ratios. Below a molar fraction of 0.5 for ammonia, his results are consistent with Donaldson's results and with the postulated ammonia–water cluster. Above 0.5 molar fraction of ammonia, an abrupt change of behavior is observed that would be best explained by the formation of a monolayer of NH_3 on the aqueous solution.

2.4. Interactions of ammonia with atmospheric water

2.4.1. In-cloud scavenging of ammonia

Shimshock and De Pena [28,29] have analyzed the mass transfer of gaseous ammonia to a raindrop using Slinn's [30] expression for the flux of gas to a drop of radius R:

$$\frac{\mathrm{d}}{\mathrm{d}t}(4\pi R^3[C_{\mathrm{gas}}]) = 4\pi R^2 K_0 \left(p_{\mathrm{gas}} - \frac{[C_{\mathrm{gas}}]}{\alpha^*}\right) \tag{18}$$

where C_{gas} is the concentration of the dissolved gas in the droplet, p_{gas} the partial pressure of the gas, K_0 the overall transfer velocity of the gas in both gas and liquid phase, and α^* is the overall solubility parameter.

In the case of ammonia, they assumed an accommodation coefficient of 1 and by considering the dissociation of ammonia in water derived the following expression for α^*:

$$\alpha^* = K_{\mathrm{H}}\left(1 + [\mathrm{H_3O^+}]\frac{K_{\mathrm{B}}}{K_{\mathrm{W}}}\right) \tag{19}$$

Because of the high solubility of ammonia in water, they assumed that the mass transfer in the liquid will be much faster than the mass transfer in the gas phase and used the following approximate equation for K_0:

$$K_0 = \frac{D\,Sh}{R} \tag{20}$$

where D is the diffusion coefficient, R the radius of the drop, Sh the Sherwood number ($=1 + 0.4(Re)^{1/2}(Sc)^{1/3}$), Re the Reynolds number, Sc the Schmidt number ($=\eta/D$), and η the kinematic viscosity of air.

Integrating Eq. (18) and solving to obtain the time, t, required for $C_{\mathrm{NH_3}}$ to increase from an initial concentration $[C_{\mathrm{NH_3}}]_{\mathrm{i}}$ to a final concentration $[C_{\mathrm{NH_3}}]_{\mathrm{f}}$ gives Eq. (21):

$$t = \left(\frac{R\alpha^*}{3K_0}\right)\ln\left(\frac{P_{\mathrm{NH_3}} - [C_{\mathrm{NH_3}}]_{\mathrm{i}}/\alpha^*}{P_{\mathrm{NH_3}} - [C_{\mathrm{NH_3}}]_{\mathrm{f}}/\alpha^*}\right) \tag{21}$$

Using Eq. (21) and the approximate values of K_0 and α^* computed from Eqs. (19) and (20), the time to reach equilibrium concentration of ammonia was computed for different droplet sizes.

The results indicate that for the very small droplets, $R =$ 10–100 μm, characteristic of cloud droplet size, the equilibrium is reached in a matter of minutes, shorter than the length of time that a typical droplet exists in the cloud. Therefore, the ammonia in cloud droplets will be in equilibrium with the concentration of ammonia in the interstitial air in the cloud. It should be noted that this conclusion is consistent with the conclusions reached through alternative approaches for analysis. For example, Ponche et al. ([21] and references therein) used a framework of analysis for mass transport limits developed by Freiberg and Schwartz [31] and concluded that for ammonia, the mass transfer process will be limited by liquid phase diffusion in the droplet and that the time to reach equilibrium for a 100 μm droplet will be 0.32 s. Although the estimates of time are very different, they both indicate that for the small diameter droplets found in clouds,

the ammonia concentration in the droplet will be in equilibrium with the ammonia partial pressure in the interstitial air in the cloud.

If the liquid water content of the cloud is known, the concentration of ammonia in the droplet can be calculated using the effective Henry law constant (Eq. (19)) using the algorithm given by Shimshock and de Pena [28].

2.4.2. Below-cloud scavenging of ammonia

For the larger drop size characteristic of rain showers, the models discussed in the preceding section indicate that the concentration of ammonia in the drop will not have reached equilibrium with the ammonia in the surrounding atmosphere by the time the drop reaches the ground. Asman [32] developed the most rigorous model of the below-cloud scavenging process. The model calculates the concentration of ammonia in the raindrop as a result of two phenomena:

(1) Uptake of gaseous ammonia at the drop surface and subsequent dissociation and liquid diffusion.
(2) Change in drop radius due to water evaporation.

The model calculates the height of the cloud base from dew point calculation as a function of relative humidity and temperature at ground level, giving Eq. (22):

$$Z_{\text{base}} = c_1 + d_1 \ln(\text{RH}(0)) \tag{22}$$

where $c_1 = -9620+62.10\text{Ta}(0), d_1 = -5254-13.43\text{Ta}(0)$, Ta(0) is the temperature at ground level in K, RH(0) the relative humidity at ground level in %, and Z_{base} is the height of cloud base in meters.

Asman selected Best's distribution function for raindrop size distribution over other published distributions for the following reasons:

- Best's distribution tends to give the smallest scavenging coefficient. Since the model assumes no vertical speed of the air through which the drops fall, the calculated scavenging coefficient will be larger than the actual scavenging coefficient. Choosing the distribution that gives the smallest estimate of the scavenging coefficient therefore yields a value closer to the actual value under real atmospheric conditions.
- The Best distribution is representative of observed distribution over a larger range of rainfall intensity than any other model.

Using these assumptions, Asman derived Eq. (23) to calculate the below-cloud scavenging coefficient λ_b:

$$\lambda_b = aI^{\text{bav}} \tag{23}$$

where I is the rainfall rate at ground level, mm h^{-1}; a: aa + bb Dg (ammonia diffusivity in air), aa: $a_0 + a_1$ RH(0); bb: $b_0 + b_1$ RH(0); bav: $\text{bav}_0 + \text{bav}_1$ RH(0)

With the following values:

- $a_0 = (4.476 \times 10^{-5}) - (1.347 \times 10^{-7})\text{Ta}(0)$;
- $a_1 = (-3.004 \times 10^{-7}) - (1.498 \times 10^{-9})\text{Ta}(0)$;
- $b_0 = 8.717 - (2.787 \times 10^{-2})\text{Ta}(0)$;
- $b_1 = (-5.074 \times 10^{-2}) - (2.894 \times 10^{-4})\text{Ta}(0)$;
- $\text{bav}_0 = (9.016 \times 10^{-2}) - (2.315 \times 10^{-3})\text{Ta}(0)$;
- $\text{bav}_1 = (4.458 \times 10^{-3}) - (2.115 \times 10^{-5})\text{Ta}(0)$.

Table 6
Below-cloud scavenging coefficient for ammonia ($T = 283$ K; RH = 85%, $Z_{\text{base}} = 292$ m)

Rainfall intensity (mm h^{-1})	Scavenging coefficient (Asman) (s^{-1})
1	0.58×10^{-4}
5	1.60×10^{-4}
15	3.1×10^{-4}
25	4.2×10^{-4}

The amount of ammonia scavenged by the rainfall can then be calculated using the concentration of ammonia in the air below the cloud, volume of atmosphere affected by the rain, and period of the rainstorm, knowing the temperature and relative humidity at ground level.

2.4.3. Validation and application of the models

Comparison of predicted scavenging coefficients with scavenging coefficients calculated from measured concentrations of ammonia in rainwater has been less than satisfying. The most extensive studies, Sperber and Hameed [33] and Shimshock and de Pena [29], fail to find a link between measured scavenging coefficients and the precipitation intensity. Both groups observed a wide range of scavenging coefficients, from less than 10^{-5} to 4.0×10^{-4} s^{-1} in Sperber's study and from 6.6×10^{-6} to 8.5×10^{-4} s^{-1} in Shimshock's study. On the positive side, the median experimental value found by Shimshock and de Pena, 1.3×10^{-4} s^{-1} is close to the mean value found by Sperber and Hameed, 1.2×10^{-4} s^{-1} (standard deviation 0.2×10^{-4}). Both are in the same range as values predicted by Asman's model (Table 6).

Discrepancies between experimental and predicted scavenging coefficients can be credited to the difficulty of achieving accurate experimental determinations due to:

- Difficulty measuring precisely the low ammonia concentrations normally present in the atmosphere (a few ppbv).
- No reliable way of differentiating between ammonium ions originating from ammonia and from scavenged ammonium salts in collected rainwater.
- Difficulty measuring actual concentrations of ammonium salt-containing particulates in the atmosphere.
- Difficulty separating contributions of in-cloud and below-cloud scavenging to the total concentration of ammonium species in collected rainwater.

The combination of these factors made experimental determinations difficult to interpret and to generalize. This point is further illustrated by the wide range of conclusions reached by the researchers estimating the proportion of the total ammonia deposition contributed by below-cloud scav-

enging: Shimshock and de Pena [29]: 10%; Meszaros and Szentimrei [34]: 26–74%; and Aneja et al. [35]: 15%.

In summary, the Asman model appears to give reasonable values for below-cloud scavenging and can be used to estimate scavenging of ammonia by raindrops at a given ground level temperature and relative humidity.

2.5. Interactions with the surface of bodies of water: "dry deposition" on river, lake, and sea surfaces

2.5.1. Framework for analysis

"Dry deposition" refers to the process by which atmospheric pollutants are removed from the atmosphere without significant interaction with atmospheric moisture such as wet deposition: removal by in-cloud and below-cloud scavenging, fog droplets, or dew. For water-soluble gases such as ammonia, dry deposition over the surface of natural bodies of water (rivers, lakes, seas) represents an important mechanism for removal from the atmosphere.

The flux of removed ammonia over a unit surface area of water is given by Eq. (24):

$$F = A[C_{NH_3}]_g V_d t \tag{24}$$

where $[C_{NH_3}]_g$ is the concentration of ammonia in the air in $\mu g\,m^{-3}$; for NH_3, $1\,\mu g\,m^{-3} = 58.8\,nmol\,m^{-3} = 1.32\,ppbv$ (nmol = nanomole = 10^{-9} mol), V_d the dry deposition velocity in $m\,s^{-1}$, t is duration of the event in s, F the flux of deposited ammonia in $kg\,m^{-2}$, and A the unit conversion constant ($=10^{-9}$).

The dry deposition velocity is really an expression of the mass transfer coefficient of ammonia from the air into the water phase. Two general approaches have been used by Shahin et al. [36] to model this mass transfer process.

2.5.1.1. Application of the film theory. The film theory posits that the overall mass transfer resistance is imposed over a thin film at the interface or at the boundary layer through which diffusion is the driving force. It follows that the mass transfer coefficient is directly proportional to the diffusion coefficient and to the thickness of the boundary layer. In the case of the surface of a natural body of water, the thickness of the boundary layer is controlled, to a large extent, by the wind speed. Several empirical relationships between the mass transfer coefficient and the wind speed have been developed for water-soluble gases such as ammonia. Based on measurements of water evaporation rate, Thibodeaux [37] derived more elementary but relatively complex expressions for the mass transfer coefficients for laminar and for turbulent flows. A critical review of this approach is presented in Shahin et al.'s paper [36].

2.5.1.2. Application of the resistance model. The resistance model is the most widely used model for atmospheric deposition processes [36,38–40]. By analogy with electrical resistances, the deposition velocity, V_d, is inversely proportional to the sum of three resistances in series:

$$V_d = \frac{1}{Ra + Rb + Rch} \tag{25}$$

where Ra is theaerodynamic resistance, i.e., resistance of transport through the turbulent surface layer, Rb the resistance for diffusion through quasi-laminar air layer in contact with the water surface, and Rch the resistance due to physicochemical phenomena occurring at the interface.

The aerodynamic resistance, Ra, depends on wind speed, atmospheric stability, and surface roughness. Typically, Ra is calculated from the wind velocity, u_z, at the reference height at which the concentration of ammonia is measured (typically 10 m above the surface), and from the friction velocity, u^*:

$$Ra = \frac{u_z}{(u^*)^2} \tag{26}$$

Several semi-empirical expressions have been developed to estimate the friction velocity from the roughness length of the surface, if known, or from the standard deviation of the wind direction. Shahin et al. [36] used this previous approach that appears best suited for incorporation in a dispersion model. The aerodynamic resistance is then given by:

$$Ra = \begin{cases} \dfrac{4}{u_{10}\sigma_\theta^2}, & \text{for neutral and stable atmospheres} \\ \dfrac{9}{u_{10}\sigma_\theta^2}, & \text{for unstable atmospheres} \end{cases} \tag{27}$$

where u_{10} is the wind velocity 10 m above the surface and σ_θ is the standard deviation of the wind direction in radians.

The boundary layer resistance, Rb, is a function of the molecular diffusion coefficient for ammonia, D ($2.09 \times 10^{-5}\,m^2\,s^{-1}$ at 283K), of the kinematic viscosity of air ($\nu = 1.47 \times 10^{-5}\,m^2\,s^{-1}$ at 283 K), and of the friction viscosity, u^*, and can be estimated by using one of several published semi-empirical relationships, such as Eq. (28):

$$Rb = \frac{2}{ku^*}\left(\frac{\nu}{DPr}\right)^{2/3} \tag{28}$$

where k is the von Karman's constant (0.4) and Pr is the Prandt number of air (0.72).

In general Rch is measured experimentally from laboratory experiments using static chambers.

2.5.2. Determination of the deposition velocity

Three major approaches have been used to measure the deposition velocity of ammonia over the surface of natural bodies of water:

(1) Laboratory determination of Rch and calculations of Ra and Rb as outlined in the preceding section [38].
(2) Field measurements of ammonium compound deposition over extended period of time [41,42].
(3) Field measurements using Water Surface Sampler (WSS) and Knife-edge Surrogate Surface (KSS) techniques [36].

Table 7
Deposition velocity of ammonia over seawater

Location	V_d (mm s^{-1})	Reference
Atlantic Basin	8–20	Quinn et al. [44]
Australia-Southern Ocean	8.3	Griffiths et al. [45]
NE Pacific	8.3	Quinn et al. [46]
North and Baltic Seas	8	Barrett [47]
North Sea	7.6	Asman et al. [48]
Tampa Bay	7	Poor et al. [42]
North Sea	2–15	Lee et al. [38]

Larsen et al. [43] have compiled all the results published so far for the deposition velocity of ammonia over seawater (Table 7).

Although the results in Table 7 appear to be relatively consistent, the values reported are averages of measurements with large uncertainties associated with them. When reported, the range of values quoted reflects the uncertainty of the measurements due principally to the difficulty of measuring very small concentrations of ammonia in the air and to the lack of easy differentiation between ammonia and ammonium species from particles when dissolved in water. These values should be regarded as order of magnitude only.

Shahin et al. [36] conducted extensive measurements and analysis of dry deposition of ammonia, nitric acid, and sulfur dioxide over water surfaces in Chicago. They used direct measurements of dry deposition using surrogate techniques. An aerodynamically designed Water Surface Sampler collects the total flux of the species considered while a Knife-edge Surrogate Surface sampler captures only the particulates from an identical air stream sample. The difference between these two measurements gives an accurate measurement of the true dry deposition of a water-soluble gas such as ammonia. Their combined data for ammonia, nitric acid, and sulfur dioxide fits the following model:

$$V_d = D^{0.5}\{(0.98 \pm 0.1)u_{10} + (1.26 \pm 0.3)\} \quad (29)$$

where D is the gas-phase diffusion coefficient of the water-soluble gas, here ammonia, and u_{10} is the wind speed 10 m above the water surface; the ±values are the 95% confidence intervals for the corresponding constants. Temperature was found to have little effect on V_d. Comparison with the predictions of Thibodeaux's film theory model found that Thibodeaux's model underestimates V_d while the empirical model based on the resistance model tends to slightly overestimate V_d (see Table 2 in Shahin's paper).

The values predicted by Eq. (29) (Table 8) are in general higher than the average values reported for seawater in Table 8. A possible explanation would be that Shahin et al. [36] used fresh water in their WSS apparatus where ammonia should be expected to be more soluble than in seawater (salting-out effect).

2.5.3. Recommendations

The dry deposition of ammonia over natural bodies of water is likely to be a significant mechanism for the removal of ammonia from the atmosphere. The data presented in the preceding sections have been determined for the very low concentrations of ammonia normally present in the atmosphere, i.e., 0.1–5 ppbv. In the case of accidental release of liquid ammonia from a tank car, the concentration of ammonia in the air will be several orders of magnitude greater than normally present in the atmosphere. The driving forces and rate limiting steps for the dry deposition of ammonia over water surfaces will be drastically different from those prevailing under normal atmospheric conditions. Therefore, it is recommended that laboratory experiments be conducted to estimate the deposition velocities of high gas-phase concentrations of ammonia over both fresh water and simulated seawater.

Table 8
Deposition velocity of ammonia on fresh water (Eq. (28))

Wind speed, u_{10} (m s^{-1})	Deposition velocity, V_d (mm s^{-1})
1	11.4
2	16.4
3	21.4
4	26.4
5	31.4
6	36.4

3. Dry deposition of ammonia over the vegetation

3.1. Mechanism of uptake of ammonia by plants

Dry deposition is a mass transfer process whereby ammonia is first transported to the surface by turbulent and molecular diffusion and then removed by adsorption or absorption at the surface. In the case of vegetation, the situation is further complicated by the role of ammonia in plant physiology. Depending on the concentration of ammonia prevailing in the atmosphere, vegetation can be either a source or a sink for ammonia. This two-way exchange of ammonia between vegetation and atmosphere has become better understood in the past few years, reconciling numerous contradictory results reported in earlier publications.

In 1980, Farquhar et al. [49] suggested growing vegetation would emit ammonia when exposed to air with a concentration of NH_3 below some "compensation point" related to the partial pressure of NH_3 in the substomatal cavities. Subsequent studies confirmed the existence of this compensation point and found its value was in the range of 0.5–4 μg m^{-3} (0.66–5.28 ppbv) with a median value between 1.5 and 2 μg m^{-3} (2–2.64 ppbv) [50–56]. Distinction can be made [57] between stomatal and canopy compensation points. The stomatal compensation point refers solely to the adsorption through the stomata, the minute openings in the epidermis of a plant through which gaseous exchange with the atmosphere takes place. Canopy compensation point includes the potential exchange of ammonia between the

whole plant surface and the atmosphere, considering that particularly at elevated humidity (RH > 70%) dew on the leaf surface can adsorb ammonia reversibly or that the waxy surface of the leaves (cuticle) can retain ammonium salt particles (nitrate, chloride) that are in chemical equilibria with the vapor of their constituents. Van Hove et al. [51] did an extensive study of the stomatal compensation point for rye grass and concluded this value varied between 0.5 and 4 $\mu g\,m^{-3}$ and was influenced mainly be temperature. The typical concentration of ammonia varying from 0.75 $\mu g\,m^{-3}$ in pristine troposphere to as much as 19 $\mu g\,m^{-3}$ in polluted air ([40] p. 37), the stomatal compensation point is generally exceeded and the vegetation acts usually as a sink for atmospheric ammonia. This will definitely be the case during a release incident.

3.2. Analysis and modeling of the dry deposition process

A resistance model similar to the one described in the preceding section for water surfaces is most commonly used to analyze the dry deposition process. The deposition velocity, V_d, is inversely proportional to the sum of three resistances in series equation:

$$V_d = \frac{1}{Ra + Rb + Rc} \quad (25)$$

where Ra is the aerodynamic resistance, i.e., resistance of transport through the turbulent surface layer, Rb the resistance for diffusion through quasi-laminar air layer in contact with the soil or vegetation surface, and Rc the canopy resistance.

Aerodynamic and laminar resistances have the same meaning and mathematical description as given in Section 2.5. The canopy resistance represents a composite of the various physico-chemical phenomena involved in the interaction of ammonia with the surface. This includes the ammonia uptake through the stomata of leaves, adsorption of ammonia by moisture of the impacted surfaces (leaves, bark), as well as the absorption and chemical transformation of ammonia with soil components [58,59]. Because of the roughness of the vegetation, canopy resistance generally dominates the process, particularly during the daytime. It is seldom possible to obtain separate values for the three component resistances of the deposition velocity and experimentally determined values for V_d are generally used (see next section). However, in some large scale modeling efforts, when a great variety of terrains had to be considered, generally accepted average values for Rc (Table 9) have been used [60].

3.3. Experimental determination of dry deposition velocity

Measurement of dry deposition velocities are usually conducted at two levels, individual plant leaves in laboratory settings and forest canopy in the field level. Hanson and Lindberg [61] published a comprehensive review of both laboratory and field dry deposition measurements for reactive nitrogen compounds, including ammonia.

Table 9
Land-dependent values for canopy resistance to ammonia mass transfer

Land type	Canopy resistance ($s\,mm^{-1}$)
Arable soil	1
Forest	0.02
Grass	0.6
Moorland	0.02
Urban	0.24

3.3.1. Leaf-level measurements

Three common approaches are used in determining the mass transfer coefficient of ammonia to exposed vegetation:

(1) *Mass balance:* vegetation (leaves, branches, whole plant) is exposed to a set concentration of ammonia in air in an environmentally controlled chamber and ammonia concentration is measured at the chamber inlet and outlet to determine ammonia uptake of the plant.
(2) *Isotopic labeling:* plant is exposed to $^{15}NH_3$ and the level of radioactive label incorporated into the plant tissue is measured.
(3) *Foliar extraction:* concentration of nitrogen species is determined in an environmentally controlled chamber in plant tissue before and after ammonia exposure.

The mass balance technique is the most widely used of the three approaches.

3.3.2. Whole canopy measurements

The whole canopy measurement approach uses micrometeorological methods based on an assumption that the vertical flux through a horizontal plane, measured at a reference level above the surface, provides the flux through the atmosphere/vegetation interface. In general, two common approaches are normally used:

(1) *The eddy correlation technique:* The eddy correlation technique measures vertical turbulent flux directly from calculations of the mean covariance between the vertical component of the wind and between the pollutant concentration. Since fast and accurate ammonia concentration measurement techniques are not available, heat fluxes and local ammonia concentration measurements are used to approximate the actual turbulent flow measurements.
(2) *The flux gradient or "profile" technique:* Using the flux gradient or "profile" technique, the flux is derived from measurements of the vertical concentration profile of ammonia and eddy exchange coefficients.

Because of the various difficulties involved in measuring in real time, extremely low concentrations of ammonia in the atmosphere, the whole canopy measurements for ammonia

Table 10
Mass transfer coefficient of NH_3 to leaf surfaces (chamber method, daytime conditions)

Plant species	NH_3 conc. ($\mu g\,m^{-3}$)	Conductance, 1/Rc ($mm\,s^{-1}$)	Reference
Fescue	341	15.3	Rogers and Aneja [63]
Soybean	37	4.4	Hutchinson et al. [64]
	170	11	Rogers and Aneja [63]
Cotton	63	2.2	Hutchinson et al. [64]
	331	6.7	Rogers and Aneja [63]
Sunflower	45	4.3	Hutchinson et al. [64]
Orchard grass	283	10.3	Rogers and Aneja [63]
Snap bean	8	6–32	Farquhar et al. [49]
	140	13	Rogers and Aneja [63]
	144	2–6	van Hove et al. [50]
	502	2–6	van Hove et al. [50]
Poplar	143	0.5–9	van Hove et al. [50]
Wheat	277	15.1	Rogers and Aneja [63]
Corn	34	6.5	Hutchinson et al. [64]
	320	3.6	Rogers and Aneja [63]

have generally been accomplished using the flux gradient method.

3.3.3. Results obtained

The reported values for the dry deposition velocity of ammonia are listed in Table 9 for whole canopy experiments and in Table 10 for leaf surface measurements. Although they are expressed in the same units, the values reported for leaf surface and for whole canopy experiments are not directly comparable because they involved different receptor areas and characterize the process at a different level of substitution. It is possible to convert the mass transfer coefficient obtained on leaf surface measurements to a true deposition velocity by multiplying it by an appropriate leaf area index (LAI) that is a representative characteristic of the plant species considered. The theoretical derivation of this LAI is complex but semi-empirical values for various plant species have been published (e.g., Hanson et al. [62]).

An inspection of the values reported in Tables 10 and 11 leads to the following conclusions:

- Deposition velocities ranging from about $4\,mm\,s^{-1}$ to about $15\,mm\,s^{-1}$ characterize annual plants of modest height and foliage crown development.
- Deposition velocities ranging from about 25–$50\,mm\,s^{-1}$ characterize forests.
- There is a large variability in the data that can be attributed to:
  - differences of experimental techniques and data analysis methodology among investigators;
  - difficulties of measuring accurately low atmospheric concentrations of ammonia;
  - influence of determining variables not controlled or averaged out in the experimental design e.g., humidity, temperature, sunlight.

In the most recent investigations, the influence of these external factors has been quantified and found to have a significant impact of the measured deposition velocities (see next section).

3.3.4. Factors influencing deposition velocities

Influence of humidity: It has long been suspected that condensed atmospheric moisture deposited on the surface of leaves constituted a potential sink for atmospheric ammonia [72–74]. Wyers and Erisman [75] have attempted to quantify the impact of the moisture deposited on leaf surfaces by considering the Canopy Water Storage (CWS) level of the forest. This value can be calculated from microwave measurement of the water content of the canopy. A canopy saturated with water (e.g., after a rainfall) has a CWS value exceeding 2 mm. A dry canopy has a CWS value of less than 0.25 mm. In between, the canopy is drying. When the canopy is saturated with water (CWS > 2 mm) the resistance to ammonia deposition is very low and therefore the deposition velocities are at their maximum, averaging about $60\,mm\,s^{-1}$. When the canopy is dry (CWS < 0.25 mm), the deposition velocity decreases exponentially with the decreasing humidity level. Sutton et al. have derived Eq. (30) from both field and laboratory measurements:

$$V_d = (50\,mm\,s^{-1}) \times \left(\exp - \left(\frac{100 - RH}{12}\right)\right) \quad (30)$$

Table 11
Deposition velocity for whole canopy

Plant/terrain	NH_3 conc. ($\mu g\,m^{-3}$)	V_d ($mm\,s^{-1}$)	Method	Reference
Alpine Tundra		13 ± 6	Gradient	Rattray and Sievering [65]
Spruce forest	0.47	26 (−125 to 201)	Gradient	Andersen and Hovmand [66]
Alpine Tundra	3.8	4	Estimate	Langford and Fehsenfeld [56]
Douglas Fir Forest	6.1	22 (S.D. 50)	Eddy correlation	Duyzer et al. [67]
Douglas Fir Forest	0.1–25	32 (median)	Gradient	Wyers et al. [68]
Douglas Fir Forest		36 (24 h average) max 50 midday min 28 night	Eddy correlation	Duyzer et al. [69]
Heathland		16	Eddy correlation	Duyzer et al. [70]
Soybean	59	6.1	Chamber	Aneja et al. [71]
Snap bean	76	4	Chamber	Aneja et al. [71]
Fescue	456	11.6	Chamber	Aneja et al. [71]
Corn	190	3.1	Chamber	Aneja et al. [71]

Table 12
Annual median deposition velocities during nighttime for ammonia on the dry canopy of coniferous forest

Year	Annual median deposition velocity ($mm\,s^{-1}$)	
	RH = 42%	RH = 95%
1993	6	100
1994	8.5	32

For a drying canopy (0.25 mm < CWS < 2 mm) the average deposition velocity would range from 50 to 60 $mm\,s^{-1}$.

These average values, extracted from Wyers and Erisman data, are only applicable to well developed coniferous forest stands. For terrains with a lower aspect ratio such as pasture, agricultural fields, wasteland with low vegetation, the deposition velocities are probably about one-third of the corresponding values for forests, according to the general trend apparent in Tables 10 and 11.

Daytime/nighttime: Deposition of ammonia on vegetation during the night is influenced by both physiological and meteorological characteristics of nighttime compared to daytime. During the night, the stomata of plants close thereby stopping ammonia uptake by plant tissues. From a meteorological standpoint, calmer air, lower temperature and therefore lower humidity during the night also affect the effectiveness of ammonia deposition when night and day situations are compared. For coniferous forests, Duyzer et al. [69] have found a clear maximum for the deposition velocity of ammonia at midday (50 $mm\,s^{-1}$) and a minimum of about 28 $mm\,s^{-1}$ during the night. Wyers and Erisman [75] documented a similar trend. These authors also quantified, for nighttime conditions, the exponential decrease of deposition velocity with decreasing humidity found by Sutton for daytime conditions (Eq. (30)). However, their values are substantially different from those reported by Duyzer et al. and the annual median deposition velocities are also variable for the two years analyzed (Table 12).

Temperature and atmospheric concentration of ammonia: In field experiments, the variability of the ammonia concentration is generally relatively small and its effect difficult to isolate. Similarly, it is difficult to separate the effect of temperature from the effect of humidity. However, under the well-controlled conditions of whole canopy chamber experiments, Aneja et al. [71] have found that the concentration of ammonia in the gas phase (from 90 to 1400 ppbv) and the temperature (from 12 to 30 °C) have a negligible impact on the deposition velocity. However, at low temperatures, the decrease in physiological activities in plants leads to a closing of the stomata and to a corresponding increase in resistance to ammonia uptake which result in deposition velocities below 5 $mm\,s^{-1}$ [73].

3.4. Conclusions—recommendations

The dry deposition of ammonia over vegetation is a complex phenomenon that is still poorly understood and difficult to determine experimentally. In the case of a massive release of ammonia in the atmosphere, the high concentration of ammonia will become the main driving force for the deposition process. Aerodynamic and gas-phase diffusion resistance will become negligible and the physico-chemical phenomena on surfaces will control deposition velocity. Given the uncertainties associated with the results in the literature and the difficulties of conducting meaningful additional experiments, we recommend the adoption of the following values for dry deposition velocities:

- For forested land:
  - maximum deposition velocity = 60 $mm\,s^{-1}$ under wet conditions and at 100% humidity;
  - apply Sutton's exponential decrease (Eq. (30)) to calculate the deposition velocity for lower relative humidity levels;
  - for nighttime conditions, the maximum deposition velocity (100% humidity) = 28 $mm\,s^{-1}$.
- For terrains with low aspect ratio vegetation: agricultural crops, pastures, tundra, wasteland:
  - maximum deposition velocity = 20 $mm\,s^{-1}$ under wet conditions and at 100% humidity;
  - influence of humidity level: use Sutton's exponential decrease for maximum deposition velocity value.
  - for nighttime conditions assume a maximum deposition velocity value of 10 $mm\,s^{-1}$ at 100% humidity.

4. Reactions of ammonia with atmospheric sulfur oxides

4.1. Reactions with sulfur dioxide

4.1.1. Products of reaction

- *Anhydrous reactions of NH_3 and SO_2:* For over a century and a half chemists have known that these two gases react readily but which products are formed has remained a subject of controversy. Becke-Goehring [76] and Meyer et al. [77] conducted a comprehensive summary of early work. A more coherent, yet complex picture emerges from recent work, once the importance of the molar ratio of the two gases is realized. Vapor pressure measurements [78,79] and spectroscopic analysis [77] lead to the following conclusions:
  - At a stoichiometric ratio of 1:1, NH_3 and SO_2 reacts according to Becke-Goehring [76] and Meyer et al. [77] according to Eq. (31) to give an adduct in the form of a yellow solid, in equilibrium with the vapor pressure of its components:

$$NH_3 + SO_2 \leftrightarrow NH_3SO_2 \tag{31}$$

$$\Delta H^\circ = 32.2\,kcal\,mol^{-1}; \quad \Delta S^\circ = 84.8\,cal\,mol^{-1}\,K^{-1}$$

  - At a stoichiometric ratio of 2:1, NH_3 and SO_2 reacts according to Eq. (32) to give an adduct in the form of

a white solid, in equilibrium with the vapor pressure of its components:

$$2NH_3 + SO_2 \leftrightarrow (NH_3)_2SO_2 \quad (32)$$

$$\Delta H^\circ = 62.2\,\text{kcal mol}^{-1};\quad \Delta S^\circ = 174.8\,\text{cal mol}^{-1}\,\text{K}^{-1}$$

The reactions of anhydrous SO_2 and NH_3 gases leading to the formation of $NH_3{\cdot}SO_2$ and/or $(NH_3)_2{\cdot}SO_2$ are completely reversible. When the gas vapor pressure is sufficiently low, the solids dissociate into their original components: SO_2 and NH_3. The equilibrium conditions, i.e., the pressure at which the solids appear are a function of temperature. For the formation of $NH_3{\cdot}SO_2$, the product of the partial pressures of the reactants at equilibrium varies from 48 $Torr^2$ at 5 °C (278.15 K) to 425 $Torr^2$ at 45 °C (318.15 K). For the formation of $(NH_3)_2{\cdot}SO_2$ the temperature dependence is steeper and the corresponding equilibrium constant increases from 225 $Torr^2$ at 5 °C (278.15 K) to 1030 $Torr^2$ at 15 °C (288.15 K) [78].

- In the presence of a stoichiometric excess of SO_2, *cis*-thionylimide, HNSO, is initially formed at low temperatures, followed by the formation of red heterogeneous $(HNSO)_x$ polymers that upon warming undergo auto-redox decomposition yielding mixtures of sulfate, sulfamic acid, dithionate, thiosulfate, polythionate, and elemental sulfur. For stoichiometric ratios between 1:1 and 2:1, mixtures of the two adducts are obtained, a situation that, together with the unrecognized influence of traces of water or oxygen, created a lot of confusion in early investigations.

- Influence of water on the reaction of NH_3 and SO_2: In 1975, Heicklen and co-workers [78,80] elucidated the critical role played by water in the distribution of products obtained from the reaction of NH_3 with SO_2. If water is present in excess of the required stoichiometric amount (Eq. (33)), both the 1:1 and 2:1 adducts react quickly to form stable ammonium sulfite. When sub-stoichiometric levels of water are present ammonium pyrosulfite, $(NH_4)_2S_2O_5$, is formed.

$$2NH_3(g) + SO_2(g) + H_2O(g) \leftrightarrow (NH_4)_2SO_3(s) \quad (33)$$

$$\Delta H^\circ = -53\,\text{kcal mol}^{-1};\quad \Delta S^\circ = -113\,\text{cal mol}^{-1}\,\text{K}^{-1}$$

4.1.2. Oxidation of SO_2 in the presence of ammonia

In 1958, Junge and Ryan [81] observed that the rate of oxidation of SO_2 by oxygen was faster when the experiment was conducted using aerosol formed from sodium chloride solution spray in a polyethylene bag than when the reaction was conducted in bulk aqueous solutions. The same observation was made when ammonia was added to the bag containing a water aerosol and SO_2. Subsequent investigations of the oxygen oxidation of SO_2 in the presence of water aerosols containing sodium chloride or sea salts [82,83] confirmed these observations. Van Den Heuvel and Mason [84] re-examined the oxidation of SO_2 in the presence of ammonia and concluded that the mass of ammonium sulfate formed was proportional to the product of the surface area of the water drops and the time of exposure. Although the potential catalysis of the reaction by trace amounts of transition metal ions, particularly manganese, could not be completely discounted [85,86], these authors concluded that the acceleration of the oxidation reaction was attributable to the special conditions existing at the surface of the liquid droplets.

Brenner and co-workers [87,88] conducted a thorough, carefully designed investigation of the oxidation of SO_2 in the presence of ammonia under simulated cloud conditions and in thin water films. They established convincingly that metal catalysis was not the reason for the increased reaction rate. Nevertheless, when ammonia was present, 80% of the SO_2 was oxidized to ammonium sulfate in less than 10 min under conditions typical for the troposphere, compared to only 1% when ammonia was excluded. Their observations also excluded the postulated formation of gas-phase products that would later deposit on surfaces, particularly the intermediate formation of ammonia-sulfur dioxide clusters in the aerosol [89]. Catalysis of the reaction by the surface of the containers used in the experiments was similarly eliminated. However, the rate of reaction was dependent on the surface-to-volume ratio of the flask and on the thickness of the water film adsorbed on the internal surface of the vessel.

The results are consistent with a reaction mechanism whereby ammonia and sulfur dioxide adsorb synergistically in the thin film of water on the vessel surface or on the skin of the water droplet. The high local concentration of the three reactants, NH_3, SO_2, and O_2 in this thin film results in a high reaction rate and conversion ratio. The conversion ratio depends on the water content of the aerosol but not on the type of aerosol (NaCl crystal, soot) used to nucleate the cloud drops. Under typical cloud conditions, in the presence of ammonia, the conversion of SO_2 to sulfate will be completed in less than 5 min, a conclusion confirmed by actual cloud water sample measurements [87].

4.2. Reaction of ammonia with sulfur trioxide, SO_3

4.2.1. Gas-phase reaction of ammonia and SO_3

Sulfur trioxide (SO_3) is produced in the atmosphere from the gas-phase oxidation of SO_2 by electronically excited oxygen, by reactive molecules (O_3, NO_2, N_2O_5), and by various radicals (OH, NO_3, HO_2, RO_2, RC(O)O, ...) ([40] pp. 165–167). Subsequent reaction with atmospheric moisture produces sulfuric acid. For a long time it was assumed that the reaction of SO_3 with water should be so fast that reaction with other atmospheric components could be neglected. However, in 1988, Wang et al. [90] found that the gas-phase reaction of SO_3 and H_2O was much slower than generally assumed, with a second-order rate constant estimated to be 5.7×10^{-15} $cm^3\,mol^{-1}\,s^{-1}$. The order of magnitude of this rate constant was later confirmed by Reiner and Arnold [91] who however, reported a lower value for the rate constant: $(1.2 \pm 0.2) \times 10^{-15}$ $cm^3\,mol^{-1}\,s^{-1}$. Reactions

with other atmospheric compounds cannot be dismissed a priori. In fact, Shen et al. [92] found that the gas-phase reaction of ammonia with SO_3 was faster than the gas-phase reaction of SO_3 with water by almost four orders of magnitude: 6.9×10^{-11} cm^3 mol^{-1} s^{-1}.

As the temperature decreases (e.g., under winter conditions), the reaction with ammonia becomes competitive with the reaction with water. For example, the two reactions are expected to have the same reaction rate at −10 °C (263.15 K) and 50% RH.

Under normal atmospheric conditions, the water concentration in the atmosphere is much higher than the concentration of ammonia and SO_3 reacts mostly with water, for example:

- At 20 °C and 100% humidity the concentration of water in air is 0.94 mol m^{-3}.
- The concentration of ammonia in clean air is typically 1 ppbv or 44.5×10^{-9} mol m^{-3} and rarely exceeds 25 ppbv in polluted air which corresponds to 1.11×10^{-6} mol m^{-3}.

Because the concentration of water is at least 6 orders of magnitudes greater than the concentration of ammonia, under normal atmospheric conditions SO_3 will react predominantly with water, not with ammonia. However, under the conditions expected during a massive release of ammonia, reaction of SO_3 with ammonia will be important.

SO_3 is a strong Lewis acid and NH_3 a good electron-pair donor. Spectroscopic studies in nitrogen matrices at 12 K have found evidence for the formation of a 1:1 adduct through the donation of the nitrogen lone electron-pair to the sulfur on the SO_3 moiety [93]. More recently, Canagaratna et al. [94], using pulsed nozzle Fourier transform microwave spectroscopy, were able to demonstrate the formation of this donor–acceptor complex and to elucidate its structure.

$$NH_3(g) + SO_3(g) \rightarrow {}^{+}H_3N - SO_3{}^{-}(g) \rightarrow H_2N - SO_3H(s) \quad (34)$$

The N–S bond length at 1.957 Å is longer by 0.186 Å than the corresponding distance in crystalline sulfamic acid (H_2N–SO_3H) and the NSO angle at 97.6° is 4.9° smaller than the corresponding angle in the crystal. These two observations suggest that the dative bond is only partially formed by donation of the lone electron pair in the gas-phase adducts. This conclusion is confirmed by the determination of the nitrogen quadrupole-coupling constant that indicates that about 0.36 electrons are transferred upon formation of the complex. Upon crystallization, the zwitterionic complex rearranges to give sulfamic acid (Eq. (34)). These results are in good agreement with predictions made from theoretical ab initio calculations [95].

Lovejoy and Hanson [96] and Lovejoy [97] have investigated in detail the kinetics of the gas-phase reaction of NH_3 and SO_3 in a nitrogen atmosphere over a wide range of temperature (280–340 K) and pressure (1.3–53 kPa), using a laminar flow reactor coupled with a chemical ionization mass spectrometer for the detection of SO_3 and sulfamic acid. The second-order rate coefficient for the NH_3 and SO_3 reaction increases with increasing concentration of the carrier gas N_2. The pressure and temperature dependence of the rate coefficient is well accounted for by the Troe formalism developed for three-body gas-phase reactions:

$$k(M) = \left[\frac{k_0(M)}{(1 + k_0(M)/k_\infty}\right] \times 0.6^y \quad (35)$$

$$y = \left[\left(\frac{1 + k_0(M)}{k_\infty}\right)^2\right]^{-1} \quad (36)$$

where M refers to the carrier gas, here nitrogen, k_0(M) is the third order rate constant when the concentration of the carrier gas tends toward zero, and k_∞ is the second-order rate constant when the concentration of the carrier gas tends toward infinity. The experimental data fit the Troe model for:

$$k_0 \text{ (cm}^6 \text{ molecule}^{-2} \text{ s}^{-1}) = (3.9 \pm 0.8) \times 10^{-30}$$

$$k_\infty \text{ (cm}^3 \text{ molecule}^{-1} \text{ s}^{-1}) = (4.7 \pm 1.4) \times 10^{-11}$$

From this model, the effective second-order rate constant for the NH_3/SO_3 reaction in 1 atm N_2 at 295 K was calculated to be 2×10^{-11} cm^3 molecule^{-1} s^{-1}.

In the same study, Lovejoy and co-workers investigate the fate of the sulfamic acid formed and concluded that the following mechanisms will control the loss of sulfamic acid in the troposphere:

- Unimolecular decomposition yielding back NH_3 and SO_3: $k_d = 9\times10^{-3}$ s^{-1} for a pressure of 1 atm and temperature of 281 K.
- Scavenging by aerosols.
- Clustering with sulfuric acid molecules and scavenging of the clusters by aerosols.

Although unimolecular decomposition dominates under the very low ammonia concentrations found under normal tropospheric conditions, sulfamic acid should be stable under the high ammonia concentrations found during massive release events.

4.2.2. Gas-phase reaction of ammonia and SO_3 in the presence of water

As mentioned in the preceding section, when formed in the atmosphere, SO_3 can in principle react with either water or ammonia. The extent of reaction with each compound will depend on the relative reaction rates and concentrations of the two species. In reality, given the strong physical and chemical affinities of these three compounds, sequential or concerted series of reactions among the three chemicals and their intermediary products will likely determine the outcome of these interactions.

Tao and co-workers [98,99] used density functional and ab initio molecular orbital calculations to investigate the structure, binding energy, and energy changes associated

with the formation and inter-conversion of the complexes and products that can conceivably occur in the SO_3, H_2O, NH_3 system. Their results suggest that the intermediate fate of SO_3 in the atmosphere depends on the relative concentrations of H_2O and NH_3 that determine whether H_2O or NH_3 is initially associated with SO_3. Under normal atmospheric conditions, where the concentration of water far exceeds the concentration of ammonia, the complex $SO_3{\cdot}H_2O$ is formed initially. In the presence of ammonia, hydrogen bonded complex $SO_3{\cdot}H_2O{\cdot}NH_3$ is first formed that quickly rearranges to yield the hydrogen-bonded H_2SO_4 NH_3 complex. A small activation energy barrier of 2.25 kcal mol^{-1} separates these two complexes. Although the complex $SO_3{\cdot}NH_3{\cdot}H_2O$ is thermodynamically more stable than the complex $SO_3{\cdot}H_2O{\cdot}NH_3$, rearrangement does not occur because of the large energy barrier (13.8 kcal mol^{-1}) between the two complexes. The hydrogen-bonded $H_2SO_4{\cdot}NH_3$ complex is further stabilized by association with two molecules of water and a rapid proton transfer leading to the formation of aqueous ammonium bisulfate: $HSO_4^- \cdot NH_4^+ \cdots 2H_2O$.

In cases where ammonia is present in excess relative to water, as would be the case for massive release of ammonia, the electron donor acceptor (EDA) complex $SO_3{\cdot}NH_3{\cdot}H_2O$ complex is formed. This cluster is thermodynamically and kinetically stable. The fate of this complex is not completely understood. As mentioned in the preceding section, it is likely to be rearranged into sulfamic acid that can either dimerize and be scavenged by aerosols, or form associations with sulfuric acid or ammonium bisulfate aerosols, if present.

4.3. Reaction of ammonia with sulfuric acid and sulfate aerosols

The existence of acidic sulfate aerosols in the atmosphere has been widely reported (see Harrison and Kitto [100] for review of relevant literature). These aerosols play an important role in influencing the earth's climate by directly scattering radiation, and indirectly, by serving as cloud condensation nuclei (CCN). Because of their importance, the mechanism of formation and growth of these aerosol particles has been extensively studied but is still incompletely understood.

4.3.1. Kinetics of ammonia reaction with sulfuric acid aerosols under controlled laboratory conditions

From a phenomenological standpoint, the interaction of ammonia with sulfuric acid–water aerosol is very similar to the interaction of ammonia with water described in Section 2.3.1 The following steps are involved:

- Diffusion of ammonia in the gas phase to the liquid surface.
- Impingement of the ammonia molecule with the liquid surface resulting either in:
  - capture and adsorption of the molecule at the surface, or
  - inelastic scattering away from the surface.

If adsorption takes place, the adsorbed molecule can either:

- desorb from the surface and return to the gas phase;
- remain adsorbed as a complex formed with solvent molecules;
- react with chemicals present at the interface to form stable products.

The products formed at the interface can then migrate by diffusion into the bulk of the liquid opening new sites for additional capture of gas-phase molecules.

Consequently, the kinetics of the overall process can be controlled by one of the following steps:

- The diffusion of the ammonia molecules in the gas phase.
- The reaction rate at the interface.
- The diffusion of the products of reaction away from the surface and into the bulk of the liquid.

Depending on the experimental conditions selected, each one of these three steps can become the rate-controlling step, a situation that was not initially anticipated and that caused a lot of confusion in the literature, for example:

- Robbins and Cadle [101] using low sulfuric acid concentration (19.7 μmol m^{-3}), stoichiometric ratios for H_2SO_4/NH_3 ranging from 0.1 to 0.48 and drop diameter ranging from 0.2 to 0.9 μm, found that the initial reaction was of first-order with respect to NH_3 concentration and drop size but that, following a few seconds, the reaction kinetics did not follow any particular order. The rate constant of the initial reaction was found to be 7.6×10^4 cm^3 mol^{-1} s^{-1} (standard deviation of 0.92×10^4) with a low activation energy of 3 kcal mol^{-1}. Because increasing ammonia partial pressure or changing the carrier gas from nitrogen to helium had no significant impact on the reaction rate, they concluded that gas-phase diffusion was not controlling and that the overall process was controlled by the rate of diffusion of the product of reaction into the bulk of the droplet. They calculated a collision efficiency of 0.1, i.e., 1 out of 10 ammonia molecules hitting the droplet surface was captured and reacted at the interface.
- The same authors [102] re-examining earlier kinetic data developed by Johnstone and Williams [103] who used larger droplets (2–5 mm), higher ammonia concentrations (1–5%, v/v), and droplets with acid concentration of up to 12% concluded that the overall reaction rate was controlled by gas-phase diffusion and that every collision of ammonia with the surface resulted in reaction.

All subsequent laboratory investigations [100,104–108] reinforce the importance of initial conditions in determining

the course of the subsequent reactions. The following general conclusions can be drawn:

- The initial reaction occurs at the gas-phase/liquid interface and is of first order with respect to both gas-phase ammonia concentration and droplet surface area.
- If the partial pressure of NH_3 is low, subsequent reactions are controlled by gas-phase diffusion.
- If the partial pressure of NH_3 is high, subsequent reaction rate is controlled by the rate of diffusion of the products of reaction into the bulk of the droplet.
- The uptake coefficient increases as a function of acid concentration and reaches unity at about 55 wt.% H_2SO_4 in the droplet.
- The nature of the product formed is a function of the stoichiometric ratio of the two reactants.

In the case of a massive release of ammonia in the atmosphere, the very high concentration of ammonia and overwhelming stoichiometric ratio of ammonia over sulfuric acid will ensure a very rapid reaction rate with sulfuric acid aerosols and formation of ammonium sulfate $(NH_4)_2SO_4$ as the only product.

4.3.2. *Reaction of ammonia with sulfuric and sulfate aerosols under normal atmospheric conditions*

Importance of this reaction: New particle formation by nucleation of gas-phase species significantly influences the size and number of tropospheric aerosols. These aerosols can affect the earth's radiation budget directly by scattering solar radiation or by indirectly serving as cloud condensation nuclei (CCN). Recently, McMurry et al. [109] and Coffman and Hegg [110] observed that the rate of formation of new nanoparticles (3–10 nm) in the troposphere of clean, remote background regions was several orders of magnitude faster than predicted by the binary theory for nucleation of sulfuric acid and water. They suggested that a ternary nucleation model involving atmospheric ammonia, $H_2SO_4{\cdot}NH_3{\cdot}H_2O$, could account for the fast initial nucleation rate. Measurements by Weber et al. [111] at a remote marine site (Mauna Loa Observatory, Hawaii) and at a remote continental site (Idaho Hill, Colorado), confirmed the inadequacy of the binary model to account for the rate of nanoparticle formation and for their formation at lower sulfuric acid concentrations than predicted by the binary model. During the First Aerosol Characterization Experiment (ACE1) conducted in the sub-Antarctic island of Macquarie, south of Australia, Weber et al. [112] measured a large number of newly formed nanoparticles directly downwind from penguin colonies (source of ammonia). Furthermore, the nanoparticle concentration was also correlated with the gas-phase concentration of sulfuric acid, firmly establishing the participation of both sulfuric acid and ammonia in the formation of these ultra small particles. Kerminen et al. [113] further showed that particle growth is driven initially by the flux of sulfuric acid, followed by thermodynamic equilibration by the more abundant water and ammonia vapors. The initial fast formation of nanoparticles is followed by a slow growth phase during which particles begin to accumulate other atmospheric contaminants such as HCl and HNO_3 together with ammonia, resulting in exponential growth to particles greater than 50–100 nm that may act both as scattering material and as cloud condensation nuclei.

Apparent reaction rates in the atmosphere: Given the low concentration of ammonia typically present in the atmosphere and given the potential presence of several acidic components in the acidic aerosols (H_2SO_4, HCl, HNO), a direct measurement of the reaction rate of ammonia with sulfuric acid in the atmosphere is very difficult. Even so, Harrison and Kitto [100] carried out this determination by measuring the conversion of NH_3 to NH_4^+ as the air mass traveled between three successive distant sampling points in rural England. They established that the sum of the concentrations $[H^+ + NH_4^+]$ as well as the ratio $[H^+ + NH_4^+]/[SO_4^{2-} + NO_3^-]$ remained constant indicating no significant ammonia input during travel. The time of travel between locations was too short (1–2 h) to permit significant formation of H_2SO_4 from SO_2 oxidation during travel. The dominant acidic species in the aerosol was $NH_4{\cdot}HSO_4$. They also found a pseudo first-order reaction rate constant for the conversion of ammonia to ammonium of $(1.5 \pm 1.3) \times 10^{-4}\,s^{-1}$ between the two first sampling points and of $(1.0 \pm 1.1) \times 10^{-4}\,s^{-1}$ between the second and third sampling points. The decrease in the apparent rate constant as the reaction progresses is consistent with laboratory observation made by Huntzicker et al. [105] and McMurry et al. [106] and was attributed to the increased resistance to neutralization related to mass transfer resistance of the products through aerosol droplets because of an approaching saturation or even crystallization of the product. The apparent reaction rate is positively correlated with the acidity of the aerosol, expressed by the $[H^+]/[NH_4^+]$ mol ratio (Eq. (37)).

$$K = 23 \times 10^{-5}\left(\frac{[H^+]}{[NH^{4+}]}\right) + 4 \times 10^{-5} \quad (r = 0.65) \quad (37)$$

These rate constants are in general agreement with other determinations of the ammonia neutralization rates in the atmosphere. Erisman et al. [114] reported an average conversion rate constant of $1.0 \times 10^{-4}\,s^{-1}$ during daytime periods and $5 \times 10^{-5}\,s^{-1}$ during nighttime periods with nitric acid being the main acidic component in the atmosphere. To make their long-range transport model fit actual atmospheric measurements, Asman and van Jaarsveld [115] used a value for k of $8 \times 10^{-5}\,s^{-1}$.

- *Products of reaction–aerosol growth:* The gas-phase reaction of ammonia and sulfuric acid can lead to three well-defined compounds depending on the molar ratio of the two reactants:
  - $NH_3/H_2SO_4 = 1$; ammonium bisulfate NH_4HSO_4
  - $NH_3/H_2SO_4 = 1.5$; letovicite $(NH_4)_3H(SO_4)_2$
  - $NH_3/H_2SO_4 = 2$; ammonium sulfate $(NH_4)_2SO_4$

These compounds are stable under atmospheric conditions. Scott and Cattell [116] investigated the stability of these ammonium sulfates between 45 and 180 °C using the ring oven technique. The behavior is a complex function of temperature and composition, specifically of the proportion of acidity in the sample, i.e., $NH_4HSO_4/(NH_4)_2SO_4$ ratio. The partial pressure of NH_3 over the solid is lowered in proportion to its acidity. For example, at 25 °C, a sample containing 99.99% $(NH_4)_2SO_4$ and 0.01% NH_4HSO_4 exhibits an NH_3 partial vapor pressure of 4×10^{-12} atmospheres while a sample containing 99% $(NH_4)_2SO_4$ and 1% NH_4HSO_4 has an NH_3 partial vapor pressure of only 4×10^{-14} atmospheres. This low vapor pressure indicates ammonium sulfate, $(NH_4)_2SO_4$, will be the most stable form of solid in the atmosphere, except for in the complete absence of ammonia, and will be the initial stable product formed by the gas-phase reaction of ammonia with sulfuric acid aerosols. During the growth of the aerosol particle by capture of additional ammonia, sulfuric acid, or water, equilibrium conditions will be established that will change the initial speciation of the condensation nuclei.

Depending on the value of the molecular ratio, x, of ammonia and sulfuric acid and depending on the trend of the humidity in the atmosphere, the particle of ammonium sulfate can be solid, liquid, or it can be solid-and-liquid. The phase diagram of the system, $(NH_4)_2SO_4$–H_2SO_4–H_2O is now well understood as shown in Fig. 2, as a result of several studies aimed at modeling the formation and growth of acidic aerosols [117–124].

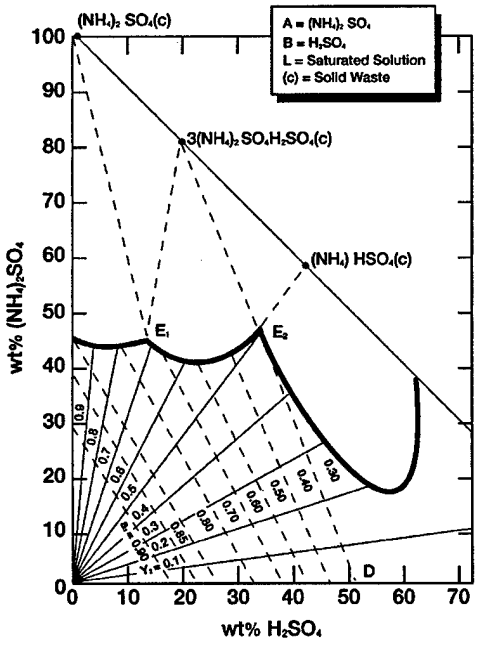

Fig. 2. Solubility diagram water–ammonium sulfate–sulfuric acid [117–119].

Depending upon the beginning composition, mixed sulfate aerosols undergo a phase transition at two distinct relative humidities that signal the onset of deliquescence for the two stoichiometric mixed crystals, ammonium bisulfate, NH_4HSO_4, and letovicite, $(NH_4)_3H(SO_4)_2$. The growth of mixed sulfate aerosol particles is best described by following the fate of a particle as a function of both increasing $x = NH_3/H_2SO_4$ and increasing relative humidity.

- For very acidic aerosol particles, $x < 1$, and low humidity, RH < 40%, the particles consist of a liquid droplet with an increased concentration of crystalline NH_4HSO_4 as x approaches 1.0, crystals appear when x reaches about 0.2 and relative humidity exceeds 20%.
- For $x = 1$ a single stage phase transition occurs at 39.5% RH and the crystalline NH_4HSO_4 particles grow to be deliquescent and commence to grow by water condensation until the crystal is fully dissolved in the water drop.
- For $1 < x < 1.5$, the droplet consists of a solid core of a mixed bisulfate and letovicite for humidity's below the deliquescent point for ammonium bisulfate, i.e., 39.5% RH. At relative humidity above 39.5% RH, the particle grows by water condensation, dissolving the bisulfate crystals and resulting in an aqueous solution of bisulfate in equilibrium with the letovicite crystals. When the RH reaches 69.3%, the deliquescence point of letovicite, a second phase transition begins to take place and the particle grows by water condensation until all the letovicite is dissolved.
- For $1.5 < x < 2$, the particle consists of a crystalline core of mixed letovicite and sulfate until the RH reaches the deliquescent point of letovicite, 69.3%, where the particle grows by water condensation and the letovicite dissolves leaving ammonium sulfate crystals in equilibrium with the solution. Ammonium sulfate deliquesces at about 80% RH.

In the case of a massive release of ammonia in the atmosphere, the stoichiometric ratio, x, will be significantly greater than two. The initial product of the gas-phase reaction of H_2SO_4 aerosols and NH_3 will be ammonium sulfate together with sulfamic acid, at a very low humidity level. For atmospheric relative humidity below 80%, nanoparticles of ammonium sulfate should be formed from reaction with pre-existing sulfuric acid aerosols together with some sulfamic acid produced by the reaction of ammonia with freshly formed SO_3 resulting from the ammonia-catalyzed oxidation of SO_2. For RH above 80%, the particles will grow by water condensation until thermodynamic equilibrium is reached for the system $[(NH_4)_2SO_4]$ solid-saturated aqueous solution–NH_3 gas. Because of the extraordinary conditions that it represents, this system has not yet been investigated. It is conceivable, however, that these particles could grow to the 50–100 nm size characteristics of cloud condensation nuclei by water condensation and/or by accretion of other products of ammonia reaction with atmospheric pollutants, for instance, ammonium nitrate and/or ammonium chloride.

5. Reaction of ammonia with atmospheric nitrogen oxides and nitric acid

Nitric oxide, NO, and nitrogen dioxide, NO_2, are primary pollutants emitted by both mobile combustion sources and emitted by stationary combustion sources. Under normal atmospheric conditions, NO is converted into NO_2 within a small number of hours. Through a variety of mechanisms involving both oxidation and hydrolysis, NO_2 rapidly ends up as either nitric acid or as peroxyacetyl nitrate (PAN) and to a slighter extent may end up as a variety of organic nitrates ([39] Chapter 8 and Section 11-B).Ammonia is known to reduce nitrogen oxides back to nitrogen. However, this reaction requires high temperatures and/or catalysts to occur at measurable rates and its occurrence under atmospheric conditions is unlikely and in fact has never been reported. To our knowledge, the reaction of ammonia with PAN has not yet been studied. It is conceivable, however, that these two chemicals would react, particularly at the surface of water droplets according to the well-known alkaline hydrolysis reaction of PAN ([39], pp. 541–542) (Eq. (38)).

$$CH_3C(=O)ONO_2 + 2NH_3 + H_2O \rightarrow NH_4CH_3CO_2 + NH_4NO_2 + \tfrac{1}{2}O_2 \quad (38)$$

To our knowledge, the presence of ammonium nitrite, NH_4NO_2, or ammonium acetate, $NH_4CH_3CO_2$, has not been reported in atmospheric aerosols. However, normal atmospheric conditions do not support simultaneous elevated concentrations of both PAN and of ammonia in the same environment. PAN tends to be predominating in urban environments, and ammonia tends to be predominating in rural environments. In the case of a massive release of ammonia in an urban environment a reaction of PAN with ammonia may possibly occur. The average concentrations of PAN range from 2 ppbv in rural environments to 70 ppbv in heavily polluted urban environments ([39], p. 369).

Aside from PAN, nitric acid is the final product for all nitrogen oxides formed in the atmosphere. Nitric acid has a great deal higher vapor pressure than does sulfuric acid under typical atmospheric conditions. It is therefore present in significant concentrations in the gas-phase rather than being present in an aerosol form, as is the case for sulfuric acid.

5.1. Gas-phase reaction of ammonia and nitric acid

The reaction of HNO_3 and NH_3 is a prototypical acid-base neutralization, i.e., proton transfer reaction, which, for all practical purposes, occurs instantaneously in aqueous solutions. However, there is no experimental evidence that this reaction takes place in the gas phase. Tao and co-workers [125,126] have used high level ab initio calculations to investigate the equilibrium structures, binding energies, and harmonic frequencies of the potential ternary clusters formed by interaction of nitric acid, ammonia, and water molecules in the gas phase. They mapped the potential energy surfaces along the proton transfer pathway to identify the preferred reaction path.

Their results indicate that in the absence of water, the nitric acid-ammonia system exists as hydrogen bonded, with nitric acid acting as the hydrogen bond donor and ammonia as the acceptor. Addition of one water molecule stabilizes the hydrogen-bonded complex but is not enough to stabilize the ion-pair that would result from proton transfer. The situations change with the addition of a second molecule of water that produces additional stabilization energy, which in turn helps stabilize the ion-pair and thus induces the transfer of a proton from the nitric acid to the ammonia to form the ammonium ion. A third water molecule contributes to further stabilization of the ion-pair.

Under normal atmospheric conditions, the concentration of water in the air is several orders of magnitudes higher than concentrations of either nitric acid or ammonia, therefore; one can expect the formation of water-stabilized ammonium nitrate clusters in the atmosphere.

5.2. Atmospheric reaction of ammonia and nitric acid

The reaction of ammonia with nitric acid yields ammonium nitrate that is in equilibrium with its gaseous constituents, whether ammonium nitrate is a crystalline solid or a solute in an aqueous solution (Eq. (39)).

$$NH_4NO_3(\text{s or aq}) \leftrightarrow NH_3(g) + HNO_3(g) \quad (39)$$

The stability of ammonium nitrate has been the object of several studies [127,128]. NH_4NO_3 does not start its well-known rapid, self-accelerating decomposition to N_2O and water until heated to 260–280 °C. Below this temperature it undergoes reversible decomposition into its components as shown in Eq. (39), whether in the form of melted salt above its melting point of 169.6 °C or in the form of a crystalline solid or aqueous solution at lower temperatures. Brandner et al. [129] extended the temperature range over which the vapor pressure above ammonium nitrate was measured and calculated heat of vaporization of 42.7 kcal mol^{-1} for the solid and 39.9 kcal mol^{-1} for the liquid, in reasonable agreement with the theoretical value of 42.1 kcal mol^{-1} computed from thermodynamic data.

By the mid 1970s, a number of sampling studies had shown that atmospheric aerosols often contained both ammonia and nitric acid. Stelson et al. [130] reviewed and analyzed these results and demonstrated that ammonia and nitric acid were found in a roughly 1:1 mole ratio and the product of their gas-phase concentration was, within experimental error, equal to the expected equilibrium constant for Eq. (39). This observation proved that ammonium nitrate existed as aerosol particulates in the atmosphere where it was in equilibrium with the vapor pressure of its constituents and it was not formed as an artifact on the filter media used to collect the particulates. These conclusions were confirmed

Table 13
Equilibrium constant for solid ammonium nitrate

Reference	Equation (Kc in ppm^2)	Kc at 273.15 K	Kc at 298.13 K	Kc at 303.15 K
Brandner et al. [129]	$\ln Kc = 62.296 - (21.510/T)$	7.16×10^{-8}	5.28×10^{-5}	1.73×10^{-4}
Stelson et al. [130]	$\ln Kc = 70.62 - (24.090/T) - 6.04 \ln(T/298.15)$	1.37×10^{-8}	3.80×10^{-5}	1.30×10^{-4}
Stelson and Seinfeld [135]	$\ln Kc = 70.78 - (24.220/T) - 6.10 \ln(T/298.15)$	9.97×10^{-9}	2.89×10^{-5}	9.9×10^{-5}

by additional measurements by Doyle et al. [131] using kilometer-length Fourier-transform infra red spectroscopy.

Nevertheless, significant problems continued to be reported with the accuracy and reliability of atmospheric aerosol nitrate concentrations. For example, Appel et al. [132] found the atmospheric concentrations of ammonia and nitric acid at Pittsburgh (CA) yielded values generally below those needed for agreement with the equilibrium constant of Eq. (39). Forrest et al. [133] demonstrated the NH_4NO_3 deposited on filter media was lost to volatilization for relative moisture below 60% but no measurable loss occurred at 100% relative humidity. To gain an improved understanding of the atmospheric behavior of ammonium nitrate Stelson and Seinfeld undertook extensive studies of the factors determining the equilibrium constant of NH_4NO_3 solid [134] and in acidic aqueous solutions [135].

5.2.1. *Influence of temperature on solid ammonium nitrate decomposition*

As shown in Table 13, the equilibrium constant, Kc, for the decomposition of solid ammonium nitrate into its constituents is a strong function of temperature. The equation developed by Stelson and Seinfeld [135] uses the most recent values for thermodynamic data and takes the heat capacities of the chemical species into account. It should therefore give the most accurate values for Kc.

5.2.2. *Influence of relative humidity on the decomposition of ammonium nitrate*

Stelson and Seinfeld [134] have critically reviewed the published experimental data on the relative humidity of deliquescence for ammonium nitrate. In general, most authors agree that at 25 °C, NH_4NO_3 deliquesces at a relative humidity of 62%. Reports for start of deliquescence at relative humidity as low as 30% [136] can probably be attributed to the presence of impurities, particularly to the presence of sodium nitrate.

The point of deliquescence is a strong function of temperature. Dingermans [137] found that experimental data for the deliquescence of NH_4NO_3 fit the least square expression shown in Eq. (40):

$$\ln(\mathrm{RHD}) = \frac{856.23 \pm 13.25}{T} + 1.2306 \pm 0.0439, \quad \mathrm{RHD}_{298.15\,\mathrm{K}} = 60.49\% \tag{40}$$

The thermodynamic derivation of the temperature dependence of the relative humidity at deliquescence yields a very similar relationship (Eq. (41)).

$$\ln(\mathrm{RHD}) = \frac{723.7}{T} + 1.7037, \quad \mathrm{RHD}_{298.15\,\mathrm{K}} = 62.24\% \tag{41}$$

Eq. (41) being on a strong theoretical footing and giving a result closer to the best defined experimental value in the normal range of atmospheric temperatures should probably be preferred.

5.2.3. *Aqueous solubility limit of ammonium nitrate*

The solubility limit of NH_4NO_3 in aqueous solution is also an inverse function of temperature. The results of Stephen and Stephen [138] give the least square regression, Eq. (42), for the dependence of the molality of the saturated aqueous solution as a function of temperature:

$$\ln(m) = \frac{-1837.3 \pm 18.00}{T} + 9.4235 \pm 0.0602, \quad m_{298.15\,\mathrm{K}} = 26.08\ \mathrm{mol\ kg^{-1}\ water} \tag{42}$$

The calculated value at 298.15 K agrees very well with the corresponding experimental value of Hamer and Wu [139]: 25.954 mol kg^{-1} water.

Stelson and Seinfeld's thermodynamic derivation, using the Hamer and Wu value for determining the integration constant, yields Eq. (43) that is very close to the experimental Eq. (42).

$$\ln(m) = \frac{-1600}{T} + 8.6228 \tag{43}$$

5.2.4. *Ammonium–nitric acid equilibrium product over aqueous ammonium nitrate solutions*

Stelson and Seinfeld [135] have made an extensive thermodynamic analysis of the NH_3–NO_3H–NH_4NO_3–H_2O system. Their conclusions can be summarized as follows:

- It is essential to consider the non-ideality of the concentrated solutions near the point of deliquescence. Failure to do so leads to an order of magnitude error on the calculation of the equilibrium product and of as much as 20% error on the calculation of the point of deliquescence.
- The product of ammonia and nitric partial pressure above the solution is inversely related to relative humidity but is virtually independent of pH for solutions with pH between 1 and 7. Below pH 1, the influence of undissociated nitric acid must be taken into account. At pH higher than 7, dissolved ammonia complicates the theoretical treatment of the solution.
- Unreactive solutes such as ammonium sulfate (see next section) lower the water vapor pressure but have no effect

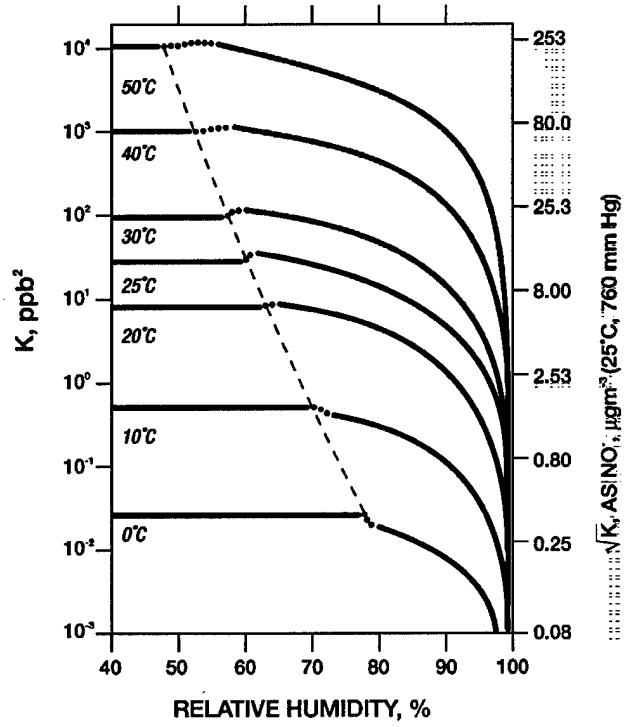

Fig. 3. Equilibrium of ammonia and nitric acid over ammonium nitrate solutions [135].

on the ammonia–nitric acid vapor pressure product. It follows that the ammonia–nitric acid vapor pressure product will be different at a given relative humidity from what it would have been at the same relative humidity in the absence of the additional solute.

The predictive equations developed by Stelson and Seinfeld are complex and have no direct application for our purpose. The overall behavior of the NH_3–NO_3H–NH_4NO_3–H_2O system is best illustrated in Fig. 3 below:

For a given temperature, the NH_4NO_3 dissociation constant is invariant below the relative humidity of deliquescence. The on-set of deliquescence occurs for increasing relative humidity as the temperature decreases. For a given temperature, above the relative humidity of deliquescence, the equilibrium constant for NH_4NO_3 dissociation decreases rapidly particularly as relative humidity approaches 100%. The discontinuity shown around the deliquescence point has several possible causes: use of different data bases for thermodynamic data for solids and solutions, errors introduced by interpolation of data, derivation of polynomial expressions for heat capacities, etc. Nevertheless, the behavior shown in Fig. 3 constitutes an accurate representation of the real behavior of the system. For example, it accounts for the observation that at 98% humidity and 25 °C, the mass concentration of NH_3 plus NO_3H in the gas in phase equilibrium with an aqueous solution of ammonium nitrate is only 1.9 $\mu g\,m^{-3}$ while 17.9 $\mu g\,m^{-3}$ would be expected if ammonium nitrate were present as a solid.

5.2.5. Kinetics of evaporation of ammonia nitrate aerosols

Larson and Taylor [140] were the first to investigate the kinetics of evaporation of NH_4NO_3 from aerosols. In their laboratory diffusion stripper, they used very small droplets (0.4 μm) of aqueous solutions of NH_4NO_3 and continuous trapping of emitted NH_3 and HNO_3. The measured rates of size reduction for the aerosol particles agreed well with those predicted from gas diffusion and concentrated solution chemistry. They concluded that the "evaporation coefficient" for both NH_3 and HNO_3 was unity, implying negligible resistance for the transport of molecules across the vapor–liquid interface.

A very different picture emerges from results obtained by later investigators particularly when actual atmospheric data were collected. Richardson and Hightower [141] levitated larger particles (2.5–3 μm) of either solid or aqueous solutions of ammonium nitrate in a vacuum in an electric quadrupole trap and observed the rate of changes of the particles' mass and size. They observed that fresh particles evaporate at a rate of $-0.23 \times 10^{-4}\,\mu m\,s^{-1}$ but that this rate decreases to $-0.06 \times 10^{-4}\,\mu m\,s^{-1}$ after 4 h. For these data to agree with thermodynamic predictions, mass accommodation coefficients (evaporation coefficients) of 0.02 must be used for the initial evaporation period, decreasing to 0.004 after 4 h. This would imply that that transport between solid and vapor phases is significantly inhibited.

Attempts to build numerical models to account for the measured concentrations of NH_3, HNO_3, and NH_4NO_3 in the atmosphere have been largely unsuccessful [142] as were attempts to identify the rate-determining step in the mechanisms involved [143]. Nonetheless, a general understanding of the factors involved emerges from several other studies [144–147] allowing a qualitative explanation of the trends observed. Deviations from predicted values based on thermodynamics occur when not enough time is available for the system to reach equilibrium after a change in the concentration of one of the chemicals involved, or after a rapid change in atmospheric conditions particularly temperature and/or relative humidity. Changes of concentrations can occur because of the proximity of a source of ammonia (cattle feedlot, chicken or pig farm) whose contribution may vary depending on wind direction [144]. Another example is the observed vertical gradient of nitric acid and nitrate aerosols. Near the ground, the rapid dry deposition of nitric acid depletes the concentration of HNO_3, triggering the decomposition of ammonium nitrate particles, an effect not observed at higher altitudes. The situation is further complicated by the presence of other anions, particularly sulfate and chlorides that compete with nitrate for ammonia. Although this general framework of interactions provides a qualitative explanation for actual atmospheric observations, the nature of the kinetic constraints preventing rapid equilibration of the system remains unknown. However, in the case of a massive release of ammonia in the atmosphere, the local high concentration of ammonia is expected to overcome any kinetic limitations and to drive the system rapidly to the com-

plete conversion of nitric acid to ammonium nitrate whose decomposition will be inhibited by the large excess of ammonia present.

5.3. Interactions of sulfuric acid, nitric acid, and ammonia in atmospheric aerosols

Ammonium sulfate and nitrate are ubiquitous components of atmospheric aerosols, having been observed in urban and rural environments in the USA and abroad (see [148] for review of relevant literature). Consequently, a substantial amount of effort has been devoted to the investigation and modeling of the NH_4NO_3–$(NH_4)_2SO_4$–NH_3–HNO_3–H_2O system.

The large difference in the stability of the two salts is one of the distinctive characteristics of this system:

$$NH_4NO_3(s) \leftrightarrow NH_3(g) + HNO_3(g), \quad K = 3.03 \times 10^{-17} \tag{44}$$

$$NH_4NO_3(aq) \leftrightarrow NH_3(g) + HNO_3(g), \quad K = 2.71 \times 10^{-17} \tag{45}$$

$$(NH_4)_2SO_4(s) \leftrightarrow 2NH_3(g) + H_2SO_4(g), \quad K = 2.33 \times 10^{-38} \tag{46}$$

$$(NH_4)_2SO_4(aq) \leftrightarrow 2NH_3(g) + H_2SO_4(g), \quad K = 2.62 \times 10^{-38} \tag{47}$$

Because of the very low dissociation constant, the dissociation of ammonium sulfate is negligible under most atmospheric conditions.

5.3.1. Thermodynamic analysis of the $NH_4NO_3/(NH_4)_2SO_4/NH_3/HNO_3/H_2O$ system

Seinfeld and co-workers [148–151] conducted a comprehensive investigation of the thermodynamics of the $NH_4NO_3/(NH_4)_2SO_4/NH_3/HNO_3/H_2O$ system, following the pioneering works of Tang [136], Seigneur et al. [152], and Tanner [153]. As could be expected from such a multi-component system, the situation is complex, particularly when attempting to build a predictive quantitative model. The two main determining variables are the molecular ratio of the ionic species (NH_4^+, NO_3^-, H^+, and SO_4^{2-}) and the relative humidity. The ratio of the ionic species determines the chemical entities present, the relative humidity determines what phase they will be present in, i.e., the phase transition from a solid particle to a liquid drop occurs when the relative humidity reaches a certain critical value corresponding to the water activity of the saturated solution. These saturated solutions have very high molality values and therefore behave in a strongly non-ideal behavior. Chan et al. [151] have demonstrated that the three models of mixed electrolyte solutions, the Zdanovskii–Stokes–Robinson (ZSR), the Kusik and Meissner (KM), and the Pitzer models, give a reasonably accurate description of the system, the ZSR model giving the most consistent prediction over the widest range of composition and relative humidity. The deviations between the prediction of the model and experimental data are attributed to the binary and ternary solute-solute interactions that are not taken into account by these models. In general, the maximum deviation does not exceed 6%. Seinfeld et al. used the KM empirical mixing rule in their thermodynamic analysis of the system. A list of temperature dependence of the various equilibrium constants and chemical potentials can be found in Basset and Seinfeld [148]. The main conclusion reached by these analyses, particularly as it applies to high concentrations of gas-phase ammonia relative to sulfuric and nitric acid concentrations (massive release of ammonia in the atmosphere), can be summarized as follows:

- Only NH_4NO_3 and $(NH_4)_2SO_4$ will be present in the liquid phase.
- As the nitrate to sulfate ratio increases from 0 to 1, the deliquescence point decreases from 80 to 62% RH at 25 °C. The decrease in the deliquescence point is small until the molecular ratio of nitrate/sulfate reaches 1/4, but accelerates thereafter, reaching about 75% RH for nitrate/sulfate ratio of 1/1, 70% RH for 3/1 until reaching the final value of 62% RH for pure ammonium nitrate as illustrated in Fig. 4. Therefore, for relative humidity below 62%, the product of reaction will be solid particles of ammonium nitrate, sulfate, or their double salts, depending on the molecular ratio of nitric and sulfuric acid in the atmosphere. Above 80%, the salts will be in the form of a liquid droplet with the salt concentration depending on the prevailing relative humidity. For relative humidity between 80% and 62% the most common occurrence will be a crystalline core particle surrounded by a saturated

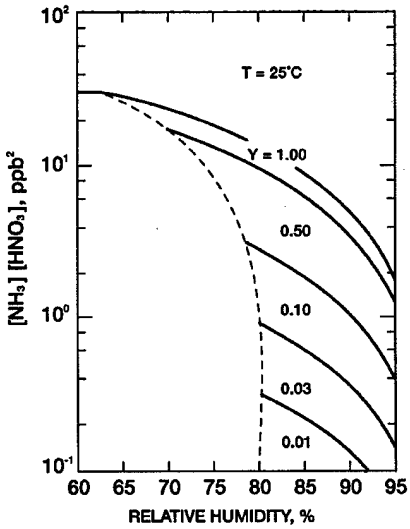

Fig. 4. The Effect of $(NH_4)_2SO_4$ on the relative humidity dependence of the NH_4NO_3 dissociation constant [149].

solution of the salts, the nature of the solid and dissolved salts depending on the nitrate-to-sulfate ratio.

- The phase diagram of the system [148] shows the formation of two double salts $2NH_4NO_3$–$(NH_4)_2SO_4$ and $3NH_4NO_3$–$(NH_4)_2SO_4$.
- As long as the high partial pressure of gas-phase ammonia persists, ammonium nitrate will not volatilize and the partial pressure of nitric acid will be negligible. When the cloud of ammonia dissipates, the ammonium nitrate will decompose into NH_3 and HNO_3 until the product of the concentration of the two gases reaches its equilibrium value for the prevailing temperature and relative humidity.

5.3.2. *Kinetics of particle growth/decay in the interactions of $NH_4NO_3/(NH_4)_2SO_4/NH_3/HNO_3/H_2O$ system*

Hightower and Richardson [154] have investigated the evaporation rate of single solid particles with initial molecular composition of 80% NH_4NO_3/20% $(NH_4)_2$ SO_4 using levitation in an electric quadrupole trap. When the evaporation was conducted in vacuum, the evaporation rate of NH_4NO_3 is as much as 360 times higher than the evaporation rate of pure, crystalline NH_4NO_3. This suggests that the mixed solid acts as a non-ideal solution, not a mixed crystal, and that the effect of sulfate is to prevent crystallization thereby causing ion mobility and mass accommodation coefficient (sticking or evaporation coefficient) to remain high. In the presence of water vapor below the deliquescence point of ammonium nitrate, 62.2% RH, the rate of NH_4NO_3 evaporation passes through a maximum for a relative humidity of about 40% at which point the evaporation rate is about 10 times faster than the evaporation rate at the deliquescent point. Although the particles do not gain any measurable weight when water vapor is introduced, Hightower and Richardson propose that the solid particle becomes coated with a superficial layer of water, a few molecules thick. The ions leave the solid and enter the water layer as fully solvated species whose evaporation rate is governed by the thermodynamics of supersaturated solutions rather than that of mixed solids. For 40% RH, the "water coating layer" would be optimal for maximum evaporation rate.

In their study of the thermodynamics of the NH_4NO_3/$(NH_4)_2SO_4/NH_3/HNO_3/H_2O$ system, Bassett and Seinfeld [150] have investigated the impact of particle size on the equilibrium state, composition, and physical state of the aerosol particles. In particular, they have considered the potential effect of the Kelvin effect that governs the vapor pressure of species in a drop as a function of the radius of the drop: the sharper the curvature of the drop, the higher the vapor pressure of the species above the drop. They concluded that the Kelvin effect had a significant impact on the distribution of the species by particle size. Ammonium sulfate being essentially non-volatile will have a size distribution controlled by gas-phase diffusion and will tend to accumulate in small size particles. Nitrates being substantially more volatile than sulfates will tend to evaporate from small particles and deposit on large particles where surface curvature effects on vapor pressure are minimal. The net effect is a mass transfer of ammonium nitrate from small to large particles and the creation of a bimodal distribution with very fine particles where ammonium sulfate predominates on one end and larger particles with a core of ammonium sulfate surrounded by deposited ammonium nitrate at the other end. This type of distribution has been observed repeatedly when sampling atmospheric aerosols (see reference [39] pp. 786–790 for review of relevant data).

As mentioned in Section 5.2, in actual atmospheric measurements, deviation from equilibrium concentrations, product phase and composition are often observed (e.g., [153,155]). These deviations are mostly due to the inability of the system to reach equilibrium after rapid changes of temperature, relative humidity, or gas-phase composition, mainly because of slow diffusion of species within the bulk of the particle [148].

6. Reaction with hydrochloric acid

The level of HCl in the troposphere is highly variable and not well documented ([39], p. 678). The main source stems from the reaction of sea-salt aerosols with strong acid aerosols such as sulfuric and nitric acids. Anthropogenic sources such as waste incineration and automobile emissions provide the balance for the observed HCl concentration in the atmosphere. Therefore, HCl should be expected to be prevalent in coastal areas but the observed levels seldom exceed the low ppb range.

6.1. *Gas-phase reaction of ammonia and hydrochloric acid*

Like nitric and sulfuric acid, hydrochloric acid is a strong acid that reacts extremely rapidly with ammonia in aqueous solutions, yielding ammonium chloride.

Early investigators using measurements of vapor densities and dissociation pressure, as well as thermodynamic calculations, concluded that in the gas phase, ammonium chloride was completely dissociated into HCl and NH_3 [156]. This commonly held view was challenged by ab initio calculation of the electronic structure of the NH_4Cl molecule predicting a minimum in the NH_4Cl potential energy surface that would be 19 kcal mol^{-1} lower than the energy of its dissociation products [157]. Shortly thereafter, Golfinger and Verhagen [158] using quadrupole mass spectroscopy provided unambiguous evidence for the presence of undissociated deuterated ammonium chloride in the vapor effusing from a Knudsen cell. Shibata [159] further demonstrated the presence of undissociated ammonium chloride in the gas phase, using electron diffraction spectroscopy. De Kruif [160] using a torsion effusion technique where electromagnetic forces are used to compensate for the recoil of vapor molecules effusing from a cell in which ammonium chloride is vaporized, determined that approximately 85% of NH_4Cl is dissociating into NH_3 and HCl in

the gas phase at 352 K (79 °C). The degree of dissociation increases only slowly with increasing temperature.

Advanced ab initio calculations by Tao and co-workers [161–164] support the formation and stability of NH_4Cl in the gas phase. The single NH_3–HCl complex is hydrogen bonded only. The proton transfer does not come about until two molecules of water are present or until at least a cluster of two NH_3–HCl complexes form. The clusters of two or four NH_3–HCl units assemble into a structure resembling the crystal structure of NH_4Cl promoting proton transfer and formation of discrete NH_4^+ and Cl^- ions. The presence of water stabilizes the ion-pair over the hydrogen-bonded NH_3–HCl complex. However, maximum stabilization promoting the proton transfer is not achieved until two molecules of water are added to the NH_3–HCl complex.

6.2. Kinetics of ammonium chloride formation and nucleation

The kinetics of formation of NH_4Cl in the gas phase is more complicated than the simple homogeneous reaction of NH_3 and HCl vapors. The particles formed grow by either of two mechanisms:

(1) By deposition of additional NH_4Cl formed by homogeneous reaction in the gas phase.
(2) By adsorption of either of the two gas-phase reagents on the solid surface followed by gas–solid reaction of the adsorbed species with the other one diffusing in from the gas phase to the surface of the particle.

The partial pressure of NH_3 and HCl must exceed a minimal critical value for particles of ammonium chloride to be formed. Twomey [165] found the partial pressure of both reagents must exceed 0.005 mm of Hg for nucleation to start. Once the threshold partial pressure is exceeded the nucleation rate increases steeply, increasing the partial pressure by a factor of 6 increases the nucleation rate by 7 orders of magnitude. In later experiments, Luria and Cohen [166] found higher values for the onset of nucleation, 3.5×10^{14} molecules cm^{-3} (0.010 mmHg) in a stationary system and four to five times higher values still in a flow system. It seems likely the critical minimal concentration for the onset of nucleation depends on experimental conditions (gas flow rates, cell geometry, temperature).

Countess and Heicklen [167] found the homogeneous bimolecular reaction rate for the gas-phase reaction was 1.9×10^{-17} cm^3 s^{-1}. The number of particles produced increases first linearly with time then levels off as the reactants, NH_3 and HCl, are consumed. Luria and Cohen [166] found the same behavior proved growth of particles does not occur by particle coagulation but rather takes place by adsorption of one of the reagents onto the particle surface followed by gas–solid reaction with the other reagent. The processes of nucleation and subsequent particle growth are described by the following kinetics equations:

$$\text{Nucleation}: R\{\text{N}\} = 10^{(-76\pm15)}\ \text{cm}^{13.2}\ \text{s}^{-1}\ [\text{NH}_3][\text{HCl}]^{2.7} \quad (48)$$

where $R\{N\}$ represents the particle production rate.

$$\text{Particle growth}: R\{\text{NH}_4\text{Cl}\} = 7 \times 10^{-26}\ \text{cm}^6\ \text{s}^{-1}\ [\text{NH}_3][\text{HCl}][\text{N}] \quad (49)$$

where $R\{NH_4Cl\}$ is the rate of NH_4Cl formation in the solid phase and [N] is the concentration of particles already formed.

There is still considerable uncertainty associated with the determination of the nucleation rate (Eq. (48)), experimental errors being magnified by the derivation of the rate constant from the slope of a log–log plot of the data.

Under normal atmospheric conditions, the partial pressure of both ammonia and HCl are below the critical minimal value for the onset of nucleation. It is therefore likely that ammonium chloride will form on the surface of existing particles where ammonia or HCl would have adsorbed. This will certainly occur in the case of a massive release of ammonia during which the high partial pressure of ammonia will drive the reaction.

6.3. Thermodynamics of ammonium chloride dissociation

Pio and Harrison [168,169] conducted a critical review and assessment of the thermodynamics of ammonium chloride decomposition. As discussed in the preceding section for ammonium nitrate, relative humidity and temperature are the two main determinants for the equilibrium constant for ammonium chloride dissociation according to Eq. (50).

$$\text{NH}_4\text{Cl(s)} \leftrightarrow \text{NH}_3\text{(g)} + \text{HCl(g)} \quad (50)$$

The point of deliquescence decreases linearly from 85% RH at −10 °C to 68% RH at 70 °C. Therefore, under normal atmospheric conditions, the deliquescence point will range from 75 to 80% RH. Below this range, NH_4Cl will be present as solid particles and above as liquid droplets of concentrated aqueous solution. Using the best available thermodynamic values in Van's Hoff equation, Pio and Harrison [168] derived Eq. (51) for the temperature dependence of the equilibrium constant for solid ammonium chloride:

$$\ln(\text{Kp}) = 2.2358\ln(T) - 2.13204 \times 10^4\, T^{-1} + 65.437516 - 8.167 \times 10^{-3} T + 4.64383 \times 10^{-7} T^2 - 1.10475 \times 10^{-10} T^3,$$
$$\text{Kp}_{298\,\text{K}} = 71.56\ \text{ppb}^2 \quad (51)$$

Values calculated using Eq. (51) are reasonably close to those of the empirical Eq. (52) derived by Wagner and Newman [170] from measurements of vapor pressure between

35 and 85 °C:

$$\ln(\mathrm{Kp}) = 1.812\ln(T) - 2.138641 \times 10^4 T^{-1} + 68.258553 - 7.4604 \times 10^{-3} T, \quad \mathrm{Kp}_{298\,\mathrm{K}} = 102.3\ \mathrm{ppb}^2 \quad (52)$$

As observed for ammonium nitrate, above the deliquescence point, the product of partial pressure of ammonia and hydrochloric acid above the aqueous droplet is much lower than the corresponding product for the solid particle below the deliquescence point. At a given temperature, the partial pressure product at 95% RH is 10–20 times lower than the corresponding product of partial pressure above the solid. Increasing RH to 98% further decreases the product 60–100 times from the value expected over the solid.

Measurements of atmospheric concentrations of NH_3, HCl, and HNO_3 in England and the Netherlands [145] revealed that in large, the measured concentrations are in agreement with those predicted for equilibrium chemical thermodynamics of a non-interactive external mixture of ammonium chloride and nitrate. Deviations are seen at low temperatures (<5 °C) and high relative humidity (>80% RH). Although no definitive explanation can be found, it is believed these deviations result from kinetic constraints preventing the system from reaching equilibrium after a rather rapid change of atmospheric conditions.

6.4. Kinetics of ammonium chloride dissociation

Harrison et al. [146] measured the evaporation rate of ammonium nitrate and chloride aerosols in an annular denuder where vapors of NH_3, HCl, and HNO_3 are rapidly and continuously removed. Rates were expressed in terms of the rate of decrease of particle diameter. The results are summarized in Table 14.

Harrison et al. [146] reached the following conclusions:

- Evaporation rates measured are independent of particle radius and low compared to those predicted by existing theories of aerosol evaporation, implying that achievement of equilibrium is hindered by some kinetic constraint. It was postulated, the low evaporation rate of NH_4Cl from the solid particle would be consistent with a mechanism where the rate limiting step would be the conversion of NH_4Cl into physically adsorbed NH_3 and HCl at the surface of the particle.
- Ammonium chloride dissociates faster than ammonium nitrate, particularly from aqueous solutions.

Table 14
Evaporation rate of ammonium chloride and nitrate aerosols

	Evaporation rate ($A\,s^{-1}$)	
	NH_4Cl	NH_4NO_3
Dry aerosol	−1.05	−0.45
Liquid aerosol	−4.52	−0.49

- For liquid droplets, the rate-limiting step could be the diffusion of the solvated ions within the liquid.
- Differences between chloride and nitrate evaporation from liquid droplets may be due to differences in deliquescence points between the two salts leading to different solute concentrations at the same RH and to a difference in concentration changes for small RH changes in the high relative humidity range.

7. Reactions of ammonia with carbon dioxide

Carbon dioxide is one of the main chemical components of the atmosphere where concentrations average 360 ppm. Gas-phase reaction of ammonia and CO_2 is not expected to occur and has never been reported under atmospheric conditions, however, in aqueous solutions, CO_2 forms carbonic acid, a weak acid that reacts with ammonia to give three possible products:

$$NH_3 + CO_2 + H_2O \leftrightarrow NH_4^+ + HCO^{3-} \quad (53)$$

$$NH_3 + NH_4^+ + HCO_3^- \leftrightarrow 2(NH_4)^+ + CO_3^{2-} \quad (54)$$

$$NH_3 + HCO_3^- \leftrightarrow NH_2COO^- + H_2O \quad (55)$$

As indicated in Eqs. (53)–(55), the species formed: ammonium bicarbonate, ammonium carbonate, and ammonium carbamate are in equilibrium with NH_3 and CO_2 vapors. Under normal atmospheric conditions, where ammonia concentrations are in the low ppb range, the contribution of these reactions is essentially negligible.

In the case of a massive release of ammonia in the atmosphere, the high partial pressure of ammonia will lead to a high concentration of dissolved ammonia in water droplets in the atmosphere as well as in any surface water in contact with the ammonia cloud. This dissolved ammonia will in turn react with atmospheric CO_2 according to Eqs. (53)–(55).

The CO_2–NH_3–H_2O system is of considerable interest in the chemical industry where it is used, for example, for the scrubbing of flue gases from coal gasification operations. The most extensive set of experimental data was developed by van Krevelen et al. [14] and has been used ever since to test various models describing the equilibrium in aqueous solutions of weak electrolytes [15,171,172].

Van Krevelen et al. [14] used a simple Setschenow correction for non-ideal solutions in which the logarithm of the activity coefficient is assumed to be a linear function of the ionic strength, to calculate empirical values for the three equilibrium constants for Eqs. (53)–(55). Using these equilibrium constants and Henry's law constants, they outlined an iterative method to calculate the composition of the aqueous solution and vapor pressure above it for a wide range of ammonia concentrations, ratio of mole-fractions of total CO_2 and total ammonia ($R = (CO_2 + CO_3H^- + CO_3^{2-} + NH_2COO^-)/(NH_3 + NH_4^+ + NH_2COO^-)$), and temperature. The resulting graph for high ammonia concentration (20 N) and 20 °C, is shown in Fig. 5.

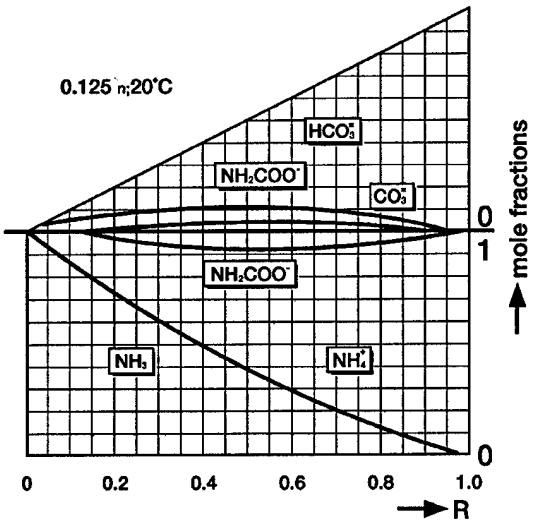

Fig. 5. Equilibrium of ammonia and carbon dioxide over aqueous solutions [14].

The upper triangle in Fig. 5 shows the speciation for CO_2, the lower rectangle shows the speciation for ammonia. For the case of massive release of ammonia, R will be close to zero. The CO_2 in solution will be present as carbonate and bicarbonate and very little if any carbamate would be expected. As long as the partial pressure of ammonia above the water surface is high, the partial pressure of CO_2 will be very small. The amount of atmospheric CO_2 trapped in solution as ammonium carbonate/bicarbonate will be limited by the rate of gas-phase diffusion of atmospheric CO_2 toward the water surface. Given that condensed water must be present and that the initial concentration of CO_2 is low, 360 ppm, the overall impact of atmospheric CO_2 on ammonia removal can be neglected for all practical purpose.

8. Reactions of ammonia with atmospheric oxidants

8.1. Reaction with hydroxyl radicals

The primary reaction of ammonia with OH radicals produces an amidogen radical, NH_2, which reacts further with other oxidative species in the atmosphere (O_2, O_3, OH, H_2O_2). This primary reaction (Eq. (56)) is the rate-determining step in the atmospheric oxidation of ammonia [173]. The subsequent reactions of the amidogen radical have not been investigated in detail but are believed to result in the formation of NO_x.

$$NH_3 + OH \rightarrow NH_2 + H_2O \quad (56)$$

Stuhl [174] conducted the first experimental determination of kinetics of Eq. (56) and found a rate constant of $1.5(\pm 0.4) \times 10^{-13}$ cm^3 molecule^{-1} s^{-1} at 298 K. Since, 18 separate determinations of this rate constant have been reported with values ranging from 0.41 to 2.7×10^{-13} cm^3 molecule^{-1} s^{-1} at room temperature. Diau et al. [173] critically reviewed these investigations and concluded that experimental conditions, particularly the use of Xe lamps instead of lasers in the flash photolysis technique to generate OH radicals and the very low pressure used could be the sources of errors. In their investigations, they used either a flash lamp or an UV laser to generate the radical reactant while avoiding the production of NH_2 by photolysis of ammonia at 200 nm. A wide range of pressure (68–504 Torr) and temperature (273–433 K) was covered to ascertain the effect of these variables. They demonstrated that the impact of photolytically-generated NH_2 was negligible under their experimental conditions and that the rate constant for Eq. (56) was $1.47(\pm 0.4) \times 10^{-13}$ cm^3 molecule^{-1} s^{-1}, in good agreement with Stuhl [174] and at least five other investigators. The Arrhenius equation for Eq. (56) is given by Eq. (57). The corresponding activation energy is 1.8 Kcal mol^{-1}.

$$k\ (\text{cm}^3\ \text{molecule}^{-1}\ \text{s}^{-1}) = (3.29 \pm 1.02) \times 10^{-12} \exp\left[\frac{-(922 \pm 100)}{T}\right] \quad (57)$$

Based on the careful selection of experimental conditions and consensus with the largest number of other independent investigations, the rate constant determined by Diau et al. is the most reliable value at this point. This value of the rate constant would place the average lifetime of ammonia in the troposphere at 34 days if oxidation by OH radicals were the only source of removal.

8.2. Reaction with ozone

Heicklen and co-workers [175,176] have shown that ammonia reacts with ozone to give crystalline NH_4NO_3 according to Eq. (58).

$$2NH_3 + 4O_3 \rightarrow NH_4NO_3 + 4O_2 + H_2O \quad (58)$$

The reaction proceeds in three major steps:

(1) *Induction period* during which no formation of ammonium nitrate is observed until the products of the concentrations of ammonia and nitric acid reaches the critical value of 5.8×10^{27} molecules cm^{-3}. During this induction period, ammonia is oxidized to nitric acid. The kinetics of this reaction is a complex function of the initial stoichiometric ratio of ammonia over ozone, of the pressure of added inert gas, and of the surface-to-volume ratio of the reaction vessel used.
(2) *Particle nucleation:* Once the critical concentrations of NH_3 and HNO_3 are reached, particle formation occurs rapidly. Analysis of the data suggests that the initial particles are crystals containing 8 monomeric units of ammonium nitrate. The nucleation is completed in less than 10 min and a particle density of about 10^5 particles/cm^3 is obtained.

(3) *Particle growth:* The analysis of the kinetics of particle growth indicates that growth by particle coagulation is negligible. The particles grow by condensation of nitric acid vapor on the preformed particles followed by reaction of the adsorbed nitric acid with ammonia (Eqs. (59) and (60)).

$$HNO_3 + C_n \leftrightarrow C_n \cdot HNO_3 \quad (59)$$

$$C_n \cdot HNO_3 + NH_3 \rightarrow C_{n+1} \quad (60)$$

The rate of particle growth is controlled by the rate of condensation of nitric acid on the ammonium nitrate particles (Eq. (59)). The rate constant for reaction 51 was found to be $1.24 \times 10^{-6}\,cm^3\,min^{-1}$.

8.3. Overall loss of ammonia by oxidation

Given the very low concentrations of OH radicals (less than 1 ppt) and ozone (20–80 ppb) in the troposphere and their relatively low reaction rates, the impact of these oxidants on a massive local release of ammonia will be negligible. The same holds true for other oxidative species such as H_2O_2 and peroxy radicals that are also present at very small concentrations.

9. Interactions with airborne organic compounds

Under atmospheric conditions, ammonia is not expected to react with most organic compounds found in the atmosphere either as a result of natural processes (methane or terpenes from conifer trees for example) or from anthropogenic sources (hydrocarbons from gasoline for example). There is no indication in the literature that atmospheric reactions of ammonia with organic compounds occur.

However, organic compounds may affect the kinetics of reaction of ammonia with water and aqueous acid droplets in the atmosphere. Rubel and Gentry [177,178] showed that organic chemicals capable of forming a film on the surface of water may have a significant effect on the rate of mass transfer and reaction of atmospheric ammonia with water and aqueous acid solutions. They found that covering an acid droplet with a monolayer of solid hexadecanol decreases the accommodation coefficient of ammonia by a factor of 10. As the monolayer expands, i.e., the area per monolayer molecule increases, the monolayer experiences a phase transition from solid to liquid state. The accommodation coefficient decreases further until the monolayer collapses as it contracts because of increased monolayer cohesion. When the monolayer collapses a rapid increase in accommodation coefficient is observed.

These observations suggest that film-forming organic compounds in the atmosphere are likely to impede the dissolution of ammonia in water and its reaction with acid aerosols. This phenomenon is not fully quantified and its occurrence is difficult to predict as it will depend on the nature of the organic compounds present in the atmosphere at a given time and place. In general, the prediction for ammonia capture by water and acid aerosols should be regarded as upper limits only, the actual amount being potentially 10 times or more lower because of the effect of film-forming organic pollutants.

10. Modeling of the atmospheric chemistry of ammonia

Attempts to include the chemistry of ammonia in atmospheric models fall into three main categories:

(1) Modeling of aerosol formation, particularly ammonium nitrate particles.
(2) Long-range modeling of ammonia and ammonium salts.
(3) Catastrophic release of ammonia from industrial operations.

10.1. Modeling of aerosol formation

These models are essentially thermodynamics analysis predicting the chemical composition and growth rate of atmospheric aerosols containing nitrates, sulfates, chlorides, ammonium and other species as a function of prevailing atmospheric conditions: temperature, relative humidity, gas-phase concentrations of the reactants. They are using the thermodynamic data discussed in Section 4 for sulfate, 4 for nitrate, and 5 for chlorides. For example, the model developed by Saxena and Seigneur [179] accounts well for the composition and phase changes of aerosol particles given ambient relative humidity and gas-phase concentration of the reactants.

Chang et al. [180] developed and used STEM-II, a Eulerian transport/chemistry model that can treat as many as 44 chemical species, 23 of which are treated by the advection–diffusion equation, while the remaining species are treated by use of pseudo-steady state thermodynamics. They applied it to predict the ammonium nitrate aerosol formation in an area of Japan, far and remote from major sources of pollution. The model predicted accurately changes in aerosol composition as relative humidity, temperature and concentrations of ammonia and nitric acid changed during the day.

Campbell et al. [181] used EQUISOV II, a model that applied thermodynamics to compute equilibrium states for species distributed among a gas phase and multiple, internally mixed, size "bins" of an aerosol phase. The model was generally successful in predicting the distribution of nitrate, chloride, sulfate, and ammonium among fine and coarse particles collected over Tampa Bay, FL.

Kramm and Dlugi [182] developed an elaborate model that combines the chemistry of ammonium nitrate formation and generally accepted description of micrometeorological phenomena (transfer of momentum, sensible heat, mass) to compute the vertical fluxes of nitric acid, ammonia, and ammonium nitrate. Specifically, they use a modified inferen-

tial approach based on constant flux approximation for conserved species (i.e., total $NH_3 + NH_4^+$ and total NO_3 – nitric acid + nitrate) and on solving the flux-gradient equation by using the best available relationships for the resistance to mass transfer of the turbulent region of the atmospheric surface layer and of the underlying thin molecular turbulent sub layer. The atmosphere-vegetation interaction is modeled using a detailed account of the various resistances: stomatal resistance and cuticular resistance of foliage, dry and wet soil resistances, etc. The model yields reasonable results for the vertical distribution of chemical species when predicting expected changes caused by meteorological or chemical concentrations. However, the final test of the model against actual field data is not possible because of the present limitation of available equipment to measure actual concentrations of ammonia, nitric acid and ammonium nitrate in real time.

10.2. Long-range transport models

A number of long-range transport models have been developed and tested in Europe to describe the migration and interactions of pollutants across national boundaries. These models generally include rate equations for the reaction of acidic pollutants with ammonia and for the dry and wet deposition of ammonia and ammonium salts. Although the general trends are generally depicted faithfully, accuracy of prediction is hampered by the lack of precise information on ammonia emission and the difficulty of assessing whether a particular area is a net source or sink for ammonia (compensation point).

Russell et al. [183] developed a model describing the formation and transport of ammonium nitrate. Their Lagrangian model takes into account the kinetics of formation of nitric acid from NO_x and the thermodynamics of the ammonium nitrate equilibrium. The main uncertainty for modeling remains the accurate description of ammonia emissions from natural and anthropogenic sources. Nevertheless, the model's predictions compare favorably with actual measurements made at El Monte, CA. It explains satisfactorily the peak of nitrate formation early in the morning when the HNO_3 produced soon after sunrise reacts with the ammonia that accumulated during the night.

Long-range transport models developed to assess the fate and transport of ammonia and ammonium ions in Europe generally include selected average dry and wet deposition velocities for ammonia and ammonium ions, thermodynamics of sulfate and nitrate formation and approximate rates for the oxidation of SO_x and NO_x in the atmosphere. Various approaches are used to describe physical dispersion of the pollutants: Lagrangian [184], simple mixing and long term averaging [185], Gaussian plume formulation for point sources and statistical long term transport [186], Eulerian for horizontal transport and Gaussian for vertical distribution [187,188]. In general, long-term trends are described satisfactorily but the main weakness remains in the lack of good data for local ammonia emission. In general, ammonia is emitted near the ground and is transported only short distances from the point of emission. Ammonium sulfate and nitrate tend to be formed at higher altitude by reaction of rising ammonia with acid pollutants emitted at higher elevation and transported often from distant point sources. The ammonium salts are transported to very distant locations.

Singles et al. [188] used a multi-layer (33 layers) model to describe the vertical mixing of ammonia emitted at ground level and selected values for deposition velocities to map ammonia/ammonium concentrations in the British Isles at a fine resolution level (5 km × 5 km). Their results were in good general agreement with measured values when available.

Apsimon et al. [189] used a Lagrangian model simulating transport of a column of air divided in a large number of horizontal layers with finer resolution near ground level to describe ammonia and ammonium concentration in one location in England during an anticyclone episode in June 1983. The trajectories of air masses bringing pollutants from continental Europe was traced back and formation of ammonium species from reactions of sulfuric and nitric acids produced by oxidation of SO_x and NO_x with ammonia produced by farming in the Netherlands was simulated. The results stress the importance of limited mixing and non-homogeneous concentrations in air masses and the corresponding delays in chemical reactions.

Dentener and Crutzen [190] built a three-dimensional global transport model for ammonia and ammonium salts with a $10° \times 10°$ resolution level. Transport is described by monthly average winds and eddy diffusion parameterization based on the standard deviations of wind from the mean. Removal of ammonia by reaction with acidic aerosols (sulfate, nitrate), wet and dry depositions, and atmospheric oxidation reactions are taken into account. Anthropogenic emissions of ammonia, mainly as a result of animal husbandry, are estimated at 30.4×10^6 tonnes N per year exceeding natural sources by a factor of two. The results show reasonable agreement with measured values except for Africa and Asia where discrepancies exist.

10.3. Catastrophic releases—modeling and simulation

Release of compressed liquefied gases following the bursting of a storage vessel follows a sequence of events that can be divided into a number of distinct phases:

- Initial flash expansion, driven by the stored internal energy, leading to the formation of a fine aerosol and considerable turbulence.
- Entrainment of ambient air due to the action of this turbulence, together with evaporation of the droplets, while the turbulence decays.
- Gravitational slumping and reduction of the rate of entrainment of air in the presence of a stabilizing density gradient.
- Turbulent dispersion due to wind.

This sequence of events is extraordinarily complex and has not so far been modeled. In general, simulation and modeling efforts have concentrated on characterizing one phase of the process to eventually build a comprehensive model of the event.

Nielsen et al. [191] reported on a series of controlled releases made as part of the European "Fladis Field Experiments". The source was a horizontal flash boiling jet with release rates of 0.25–0.5 kg s^{-1}. The experimental site was heavily instrumented with five different sensor types for ammonia concentration (catalytic combustion, electrochemical, UV ionization, sonic anemometers with thermocouples, and back-scatter Lidar), numerous temperature measurements, wind speed and direction, humidity measurements, and turbulence measurements. These measurements gave a good characterization of the release as it evolves from a two-phase jet to a plume with passive dispersion. The plume was characterized by its centerline concentration, height, and width and the results compared with the prediction of several dispersion models and wind-tunnel simulations. The concentration field was analyzed in a fixed frame of reference as well as in a frame of reference moving with the instantaneous plume centerline. In general, the moving-frame statistics are in better agreement with the prediction of the dispersion models than the fixed-frame statistics of the field measurements. Source measurements of exit pressure and temperature allow estimates of release enthalpy and jet flow force. Evidence for heat input from the ground was found because of the deviation of specific plume enthalpy near the ground from expected adiabatic mixing of air and ammonia. No sign of plume lift-off was observed. Lidar measurements demonstrated the high variability of instantaneous horizontal plume profile. Small-scale turbulence within the plume adds to plume meandering caused by wind shifts to cause these concentration fluctuations. In general, the dispersion models used fail to describe plume meandering and the effect of terrain topography (slope for example) and nearby obstacles (e.g., buildings).

Deaves et al. [192] developed a mathematical model known as airborne concentration estimate (ACE) to describe the initial phase of the catastrophic release to complement the standard dispersion models. The ACE model consists of an explosion and of a turbulent growth sub-model. The explosion sub-model takes as inputs the material type, liquid mass, storage and ambient temperature and pressure before explosion and calculates the cloud radius, temperature, masses of ammonia and air, and turbulent velocity and length scale at the end of the explosion phase, i.e., when the main agent of cloud expansion changes from outward momentum provided by the explosion to air entrainment due to inherent violent turbulence. The turbulent growth sub-model describes turbulence decay from its level at the end of the explosion phase to a level comparable to the sum of atmospheric turbulence and turbulence due to gravitational slumping. Parameters in the sub-model are adjusted to fit data obtained from small-scale experiments. An energy balance is established tracking the internal energy, kinetic energy, and work done between the initial stage and the end of each phase. Liquid and gas mixture are assumed to be in equilibrium throughout the evaporation process. The model was applied to a range of catastrophic releases, illustrating the impact of the nature of the compressed liquid (chlorine, propane, or ammonia), of the release size (10–100 tonnes), and of the release direction (upward or downward) on the size and composition of the cloud, aerosol, and liquid pool as well as distance traveled and time before slumping.

11. Conclusion—recommendations

The atmospheric chemistry of ammonia has been extensively studied during the past 25 years. Being the only basic chemical naturally present in the troposphere, ammonia plays an important role in the neutralization of acidic pollutants such as nitrogen and sulfur oxides and thus impacts acid rain precipitation. On the negative side, the products of these neutralization reactions, ammonium sulfates and nitrate principally, are the main particulate components of smog and thus significantly affect the opacity of the atmosphere and the earth radiation budget while influencing precipitation events by serving as cloud condensation nuclei.

Although the results reported in the literature for the reaction of ammonia with atmospheric components are directly applicable to the case of a massive release of ammonia in the atmosphere, an important qualifier should be kept in mind. In the troposphere, ammonia is present at very low concentrations, ranging from 1 ppb in clean environments to 10–25 ppb in polluted atmosphere. In the event of a massive release of ammonia, the concentration of ammonia will be several orders of magnitude greater than considered in the reported studies. Whereas the impact of this increased concentration can be easily accounted for by using the reaction rates and equilibrium constants determined in the literature, phenomena controlled by mass transfer steps will require careful reconsideration. For example, the mass transfer of ammonia from the gas phase to the surface of water controls the rate of capture of ammonia by water under normal atmospheric conditions, because of the very low ammonia concentration in the gas phase. Under conditions prevailing during a massive release of ammonia in the atmosphere, mass transfer from gas to liquid surface will not be the rate-limiting step anymore because of the high ammonia concentration in the gas phase. Under process steps such as the diffusion of dissolved ammonia from the surface to the bulk of the liquid may become the rate-determining step.

Ammonia readily dissolves in water where it is partially hydrolyzed to ammonium hydroxide with an equilibrium constant $K_b = 1.774 \times 10^{-5}$ at 25 °C. Henry's law governs the vapor pressure of ammonia over its aqueous solutions with a constant K_H that is a function of absolute temperature

given by the following equation:

$$\ln(K_H) = -8.09694 + \left(\frac{3917.507}{T}\right) - 0.00314T$$

The application of Henry's law requires the calculation of the activity of dissolved ammonia. In dilute aqueous solutions, the activity of ammonia can be set equal to its molality without significant loss in accuracy. However, in concentrated solutions as may be found in cloud droplets or for aqueous solutions containing significant concentrations of salts, such as seawater, the activity coefficient is best computed by using the Pitzer model that takes into account the interaction of ammonia with dissolved ions and neutral molecules. Recommended values for the corresponding interaction parameters are listed in Table 5 of the paper.

As mentioned earlier, mass transfer phenomena generally control the interaction of ammonia and water in the environment and a general quantitative description of the process is still the object of some controversy. Nevertheless, to model the interaction of ammonia with water in the environment, it is useful to consider the following separate cases:

- *In-cloud scavenging of ammonia:* For the very small drop size characterizing droplets within clouds, equilibrium is quickly established between gas phase and liquid phase and the concentration of ammonia in-cloud droplets can be calculated from Henry's law.
- *Below-cloud scavenging:* Raindrop sizes are significantly larger than in-cloud droplets and their fall is too short for equilibrium to be established. Asman has developed a model (Section 2.4.2) that calculates the amount of ammonia scavenged by rainfall given the temperature and relative humidity at ground level, the concentration of ammonia below the cloud, the volume of atmosphere affected by the rain, and the duration of the rainstorm.
- *"Dry deposition" on ammonia on river, lake, and sea surfaces:* The dry deposition of ammonia over natural bodies of water is likely to be a significant mechanism for ammonia removal from the atmosphere. Available data are limited to the very low ammonia concentrations normally present in the atmosphere and for which gas-phase diffusion is the controlling process. For the high gas-phase concentrations of ammonia expected from massive release incidents, the rate-determining step is likely to be very different. Relevant data are not available in the literature. We recommend performing a series of experiments to determine the deposition velocity of ammonia over surfaces of water and seawater in the concentration range expected in the case of massive release of the gas.

The dry deposition of ammonia over vegetation is a complex phenomenon that is still poorly understood and difficult to determine experimentally. In the case of a massive release of ammonia in the atmosphere, the high concentration of ammonia in air will become the main driving force for the deposition process. Aerodynamic and gas-phase diffusion resistance will become negligible and the physico-chemical phenomena on surfaces will control deposition velocity. Given the uncertainties associated with the results in the literature and the difficulties of conducting meaningful additional experiments, we recommend the adoption of the following values for dry deposition velocities:

- For forested land:
  - maximum deposition velocity = 60 mm s^{-1} under wet conditions and at 100% humidity;
  - apply Sutton's exponential decrease (Eq. (30) in Section 3.3.4) to calculate the deposition velocity for lower relative humidity levels;
  - for nighttime conditions, the maximum deposition velocity (100% humidity) = 28 mm s^{-1}
- For terrains with low aspect ratio vegetation: agricultural crops, pastures, tundra, and wasteland:
  - maximum deposition velocity = 20 mm s^{-1} under wet conditions and at 100% humidity;
  - influence of humidity level: use Sutton's exponential decrease for maximum deposition velocity value;
  - For nighttime conditions assume a maximum deposition velocity value of 10 mm s^{-1} at 100% humidity.

As mentioned earlier, ammonia is the only basic species present in the atmosphere to neutralize acidic pollutants such as sulfur and nitrogen oxides, thus mitigating the adverse effect of acid rain. Despite the low concentrations of ammonia (1–25 ppb), NO_x (0.1–750 ppb), SO_x (1–200 ppb), HNO_3 (1–25 ppb) present in the atmosphere, the neutralization reactions are rapid and reach completion or equilibrium concentration given sufficient atmospheric mixing. In the case of a massive release of ammonia, the very large stoichiometric excess of ammonia over the acidic species will ensure rapid, complete reaction resulting in the neutralization of all acidic pollutants encountered as the ammonia cloud expands. The net results will be:

- *Rapid oxidation of SO_2 to SO_3:* Ammonia was found to catalyze the oxidation of SO_2 to SO_3 under atmospheric conditions. Under normal atmospheric conditions, the reaction is complete in less than 5 min.
- *Neutralization of SO_3 by ammonia:* At very low humidity levels, ammonia will react rapidly with SO_3 to form crystalline particles of sulfamic acid. At higher humidity levels, aerosols of ammonium sulfates will be formed. For the high ammonia concentrations expected from massive release incidents, neutral ammonium sulfate, $(NH_4)_2SO_4$, is expected to be the main product formed. At relative humidity below 80%, nanoparticles of ammonium sulfate will predominate with possibly some sulfamic acid. Above 80% humidity, the ammonium sulfate particles will grow by water condensation until thermodynamic equilibrium is reached for the system $[(NH_4)_2SO_4]$ solid-saturated aqueous solution–NH_3 gas.
- *Neutralization of nitric acid formed by atmospheric oxidation of NO_x:* The reaction is very rapid and leads to the production of ammonium nitrate that tends to de-

posit on pre-existing ammonium sulfate nanoparticles, resulting in the formation of aerosols of coarser particles (10–100 μm). Under normal atmospheric conditions, ammonium nitrate is in equilibrium with the vapor pressure of its constituents, NH_3 and NO_3H. However, with the high gas-phase concentration of ammonia expected during massive release incidents, ammonium nitrate will be stable. The physical form and chemical composition of the aerosol is a complex function of the relative humidity and of the sulfate-to-nitrate ratio (Section 5.3).

- *Neutralization of hydrochloric acid:* This reaction is expected to be significant in marine environments where HCl is formed by reaction of sea-salt aerosols with strong acid aerosols such as sulfuric and nitric acids. The reaction is very fast and results in the formation of ammonium chloride. Like ammonium nitrate, ammonium chloride contributes to the growth of ammonium sulfate particles and is in equilibrium with the partial vapor pressure of its constituents. While high gas-phase concentrations of ammonia are prevailing, ammonium chloride is expected to be stable.
- *Neutralization of carbon dioxide:* To react with ammonia, CO_2 must be dissolved in water and ionized as carbonate or bicarbonate ions. The amount of atmospheric CO_2 trapped in solution, as ammonium carbonate/bicarbonate will be limited by the gas-phase diffusion of atmospheric CO_2 toward the water surface. Given that condensed water must be present and that the initial concentration of CO_2 is low, 360 ppm, the overall impact of atmospheric CO_2 on ammonia removal can be neglected for all practical purpose.

In summary, the acidic pollutants in the atmosphere will react very rapidly with ammonia present at high concentration resulting in the formation of ammonium salt aerosols that will increase the opacity of the atmosphere locally. From a modeling standpoint, these acidic components of the atmosphere can be considered as a sink for ammonia, removing a stoichiometric amount of ammonia as the cloud of released gas travels through the atmosphere. It should be noted that no data was uncovered for the kinetics of reaction of ammonia with peroxyacetyl nitrate a common component of polluted atmospheres. PAN is known to hydrolyze in alkaline solutions, forming acetate and nitrate salts. Given the low concentrations of PAN in the troposphere (2–70 ppb), it might be reasonable to assume that PAN constitutes another sink for ammonia through alkaline hydrolysis in ammonia saturated water droplets.

Ammonia reacts relatively slowly with OH radicals in the atmosphere where its average lifetime would be 34 days if oxidation by OH radicals were the only source of removal. This pathway of ammonia removal can therefore be neglected. The reaction with ozone is very rapid for high concentration of ammonia and results in the formation of ammonium nitrate. Given the low concentration of ozone in the atmosphere (80 ppb), ozone can be considered as another small sink for ammonia, as suggested for atmospheric acidic components.

Several models, incorporating the chemistry of ammonia in various degrees, have been developed to account for the long-range transport of ammonium species in the atmosphere. In general, ammonia is only transported to short distances from the emission source because of efficient scavenging by water and vegetation. Ammonium salts on the other hand are transported over longer distances. Limited information on the modeling and on actual trials of catastrophic release of ammonia from storage tanks stress the importance of physical and thermo dynamical processes during the actual tank rupture on the volume and shape of the dense plume formed. Additional research in this area is critical to the development of a realistic model of massive release of compressed liquefied gas from ruptured containment vessels.

Acknowledgements

The financial support of the Defense Threat Reduction Agency (DTRA) is gratefully acknowledged.

References

[1] R.G. Bates, G.D. Pinching, J. Res. Nat. Bur. Stand. 72 (1950) 1393.
[2] S.L. Clegg, P. Brimblecombe, J. Phys. Chem. 93 (1989) 7237.
[3] M. Eigen, J. Schoen, Z. Elektrochem. 59 (1955) 483.
[4] M. Eigen, Angew. Chem. Int. Ed. (Engl.) 3 (1964) 1.
[5] M.T. Emerson, E. Grunwald, R.A. Kromhout, J. Chem. Phys. 33 (1960) 547.
[6] J.M. Hales, D.R. Drewes, Atmos. Environ. 13 (1979) 1133.
[7] T.J. Edwards, G. Maurer, J. Newman, J.M. Prausnitz, Am. Inst. Chem. Eng. J. 24 (1978) 966.
[8] P.K. Dasgupta, S. Dong, Atmos. Environ. 20 (1986) 565.
[9] Q. Shi, P. Davidovits, J.T. Jayne, D.R. Worsnop, C.E. Kolb, J. Phys. Chem. A 103A (1999) 5160.
[10] National Bureau of Standards—Selected Values of Chemical Thermodynamic Properties, Circular 500, Washington, DC, 1952.
[11] D.D. Wagman, W.H. Evans, V.B. Parker, I.H. Schumm, S.M. Bailey, K.L. Churney, R.L. Nuttall, J. Phys. Chem. Ref. Data 11 (1982) 1.
[12] Q. Shi, P. Davidovits, J.T. Jayne, D.R. Worsnop, C.E. Kolb, J. Phys. Chem. A 103A (1999) 5160.
[13] H.A. Laitinen, W.E. Harris, Chemical Analysis, McGraw-Hill, New York, 1975.
[14] D.W. van Krevelen, P.J. Hoftijzer, F.J. Huntjens, Recl. Trav. Chim. Pays-Bas 68 (1949) 191.
[15] C.C. Chen, H.I. Britt, J.F. Boston, L.B. Evans, Am. Inst. Chem. Eng. J. 25 (1979) 820.
[16] K.S. Pitzer, Rev. Mineral 17 (1987) 97.
[17] N.A. Fuchs, A.G. Sutugin, Highly Dispersed Aerosols, Ann Arbor Science Publishers, Ann Arbor, 1970.
[18] V.V. Larson, G.S. Taylor, Atmos. Environ. 17 (1983) 2489.
[19] C.B. Richardson, R.L. Hightower, Atmos. Environ. 21 (1987) 971.
[20] R.M. Harrison, W.T. Sturges, A.M. Kitto, Y. Li, Atmos. Environ. 24A (1990) 1883.
[21] J.L. Ponche, C. George, P. Mirabel, J. Atmos. Chem. 16 (1993) 1.
[22] A. Bongartz, S. Schweighoefer, C. Roose, U. Schurath, J. Atmos. Chem. 20 (1995) 35.
[23] P. Davidovits, J.T. Jayne, S.X. Duan, D.R. Worsnop, M.S. Zahniser, C.E. Kolb, J. Phys. Chem. 95 (1991) 6337.

[24] Q. Shi, P. Davidovits, D.R. Worsnop, J.T. Jayne, C.E. Kolb, J. Phys. Chem. 103 (1999) 8812.
[25] D.J. Donaldson, J. Phys. Chem. 103 (1999) 62.
[26] D. Simonelli, M.J. Schultz, J. Chem. Phys. 112 (2000) 6804.
[27] N.G. McDuffie, Langmuir 17 (2001) 5711.
[28] J.P. Shimshock, in: Presented at the Second International Specialty Conference on Meteorology of Acidic Deposition, Air Pollution Control Association, Pittsburgh, PA, 1986, p. 402.
[29] J.P. Shimshock, R.G. De Pena, Tellus 41B (1989) 296.
[30] W.G.N. Shinn, USDOE Office of Scientific and Technical Information, Oak Ridge, 1984, p. 466.
[31] J.E. Freiberg, S.A. Schwartz, Atmos. Environ. 15 (1981) 1145.
[32] W.A.H. Asman, Atmos. Environ. 29 (1995) 1359.
[33] K.R. Sperber, S. Hameed, J. Geophys. Res. 91 (1986) 11833.
[34] E. Meszaros, T. Szentimrei, J. Atmos. Chem. 2 (1985) 405.
[35] V.P. Aneja, A.B. Murthy, W. Battye, R. Battye, W.G. Benjey, Atmos. Environ. 32 (1998) 353.
[36] U.M. Shahin, T.M. Holsen, M. Odabasi, Atmos. Environ. 36 (2002) 3267.
[37] L.J. Thibodeaux, Chemodynamics: Environmental Movement of Chemicals in Air, Water, and Soil, Wiley, New York, 1979.
[38] D.S. Lee, C. Halliwell, J.A. Garland, G.J. Dollard, R.D. Kingdon, Atmos. Environ. 32 (1998) 431.
[39] B.J. Finlayson-Pitts, J. Pitts, James N., Atmospheric Chemistry: Fundamentals and Experimental Techniques, Wiley, New York, 1986.
[40] J.H. Seinfeld, Atmospheric Chemistry and Physics of Air Pollution, Wiley, New York, 1986.
[41] P.K. Quinn, R.J. Charlson, W. Zoller, H., Tellus 39B (1987) 413.
[42] N. Poor, R. Pribble, H. Greening, Atmos. Environ. 35 (2001) 3947.
[43] R.K. Larsen III, J.C. Steinbacher, J.E. Baker, Environ. Sci. Technol. 35 (2001) 4731.
[44] P.K. Quinn, K. Barrett, F.J. Dentener, F. Lipschultz, K.D. Six, Biogeochemistry 35 (1996) 275.
[45] F.B. Griffiths, T.S. Bates, P.K. Quinn, L.A. Clementson, J.S. Parslow, J. Geophys. Res.-Atmos. 104 (1999) 21649.
[46] P.K. Quinn, R.J. Charlson, T.S. Bates, Nature 335 (1988) 336.
[47] K. Barrett, Atmos. Environ. 32 (1998) 381.
[48] W.A.H. Asman, R.M. Harrison, C.J. Ottley, Atmos. Environ. 28 (1994) 3647.
[49] G.D. Farquhar, P.M. Firth, R. Wetselaar, B. Weir, Plant Physiol. 66 (1980) 710.
[50] L.W.A. van Hove, A.J. Koops, E.H. Adema, W.J. Vredenberg, Atmos. Environ. 21 (1987) 1759.
[51] L.W.A. van Hove, P. Heeres, M.E. Bossen, Atmos. Environ. 36 (2002) 2965.
[52] S.M. Dabney, D.R. Bouldin, Atmos. Environ. 24 (1990) 2655.
[53] L.A. Harper, R.R. Sharpe, G.W. Langdale, J.E. Giddens, Agron. J. 79 (1987) 965.
[54] J.K. Schjoerring, Trace Gas Emissions by Plants, Academic Press, San Diego, 1991.
[55] S. Hamstein, M. Mattson, H.J. Jaeger, J.K. Schjoerring, New Phytol. 141 (1999) 71.
[56] A.O. Langford, F.C. Fehsenfeld, Science 255 (1992) 581.
[57] M.A. Sutton, J.K. Burkhardt, D. Guerin, E. Nemitz, D. Fouler, Atmos. Environ. 12 (1998) 473.
[58] R.B. Hanawalt, Soil Sci. Soc. Am. J. 33 (1969) 231.
[59] R.B. Hanawalt, Soil Sci. Soc. Am. J. 33 (1969) 725.
[60] R. Singles, M.A. Sutton, K.J. Weston, Atmos. Environ. 32 (1998) 393.
[61] D.R. Hanson, S.E. Lindberg, Atmos. Environ. 25A (1991) 1615.
[62] P.J. Hanson, K. Rott, G.F. Taylor, C.A. Gunderson, S.E. Lindberg, B.M. Ross-Todd, Atmos. Environ. 23 (1989) 1783.
[63] H.H. Rogers, V.P. Aneja, Atmos. Environ. 20 (1980) 251.
[64] G.L. Hutchinson, R.J. Millington, D.B. Peters, Science 175 (1972).
[65] G. Rattray, H. Sievering, Atmos. Environ. 35 (2001) 1105.
[66] H.V. Andersen, M.F. Hovmand, Atmos. Environ. 27A (1993) 189.
[67] J.H. Duyzer, H.L.M. Verhagen, J.H. Westrate, F.C. Bosveld, A.W.M. Vermetten, Atmos. Environ. 28 (1994) 1241.
[68] G.P. Wyers, A.T. Vermeulen, J. Slanina, Environ Pollut 75 (1992) 25.
[69] J.H. Duyzer, H.L.M. Verhagen, J.H. Westrate, F.C. Bosveld, Environ. Pollut. (1992) 3.
[70] J.H. Duyzer, A.M.H. Bouman, H.S.M.A. Diederen, R.M. van Aalst, MT-TNO Report R87/273, Delft, The Netherlands, 1987.
[71] V.P. Aneja, H.H. Rogers, E.P. Stahel, JAPCA J. Air Waste Manage. 36 (1986) 1338.
[72] L.W.A. van Hove, W.J. Vredenberg, E.H. Adema, Atmos. Environ. 24A (1990) 1263.
[73] J.W. Erisman, G.P. Wyers, Atmos. Environ. 27A (1993) 1937.
[74] M.A. Sutton, J.K. Schjorring, G.P. Wyers, Phil. Trans. R. Soc. Lond. 351 (1995) 261.
[75] G.P. Wyers, J.W. Erisman, Atmos. Environ. 32 (1998) 441.
[76] M. Becke-Goehring, Adv. Inorg. Rad. Chem. 2 (1960) 159.
[77] B. Meyer, B. Mulliken, H. Weeks, Phosphorus Sulfur 8 (1980) 291.
[78] R. Landreth, R.G. de Pena, J. Heicklen, J. Phys. Chem. 78 (1974) 1378.
[79] W.D. Scott, D. Lamb, J. Am. Chem. Soc. 92 (1970) 3943.
[80] I.C. Hisatsune, J. Heicklen, Can. J. Chem. 53 (1975) 2646.
[81] C.E. Junge, T.G. Ryan, Q. J. R. Meteorol. Soc. 84 (1958) 46.
[82] A.G. Clarke, P.T. Williams, Atmos. Environ. 17 (1983) 607.
[83] D.F. Miller, D. Lamb, A.W. Gerther, Atmos. Environ. 21 (1987) 991.
[84] A.P. van den Heuvel, B.J. Mason, Q. J. R. Meteorol. Soc. 89 (1963) 271.
[85] T.V. Larson, N.R. Horike, H. Harrison, Atmos. Environ. 12 (1978) 1597.
[86] L.R. Martin, Oxidation Mechanisms, Butterworth, Boston, 1984.
[87] A.D.A. Hansen, W.H. Benner, T. Novakov, Atmos. Environ. 25A (1991) 2521.
[88] W.H. Brenner, B. Ogorevc, T. Novakov, Atmos. Environ. 26A (1992) 1713.
[89] R.G. Keesee, K. Kilgore, J.J. Breen, J. Castleman, Aerosol Sci. Tech. 6 (1987) 71.
[90] X.Y.G. Wang, M. Suto, L.C. Lee, H.E. O'Neal, J. Chem. Phys. 89 (1988) 4853.
[91] T. Reiner, F. Arnold, J. Chem. Phys. 101 (1994) 1399.
[92] G. Shen, M. Suto, L.C. Lee, J. Geophys. Res. 95 (1990) 13981.
[93] C.J. Sass, B.S. Ault, J. Phys. Chem. 90 (1986) 1547.
[94] M. Canagaratna, J.A. Phillips, H. Goodfriend, K.R. Leopold, J. Am. Chem. Soc. 118 (1996) 5290.
[95] M.W. Wong, K.B. Wiberg, M.J. Frisch, J. Am. Chem. Soc. 114 (1992) 524.
[96] E.R. Lovejoy, D.R. Hanson, J. Phys. Chem. 100 (1996) 4459.
[97] E.R. Lovejoy, J. Phys. Chem. 101 (1997) 4950.
[98] L.J. Larson, A. Largent, F.-M. Tao, J. Phys. Chem. 103 (1999) 6786.
[99] L.J. Larson, F.-M. Tao, J. Phys. Chem. 105 (2001) 4344.
[100] R.M. Harrison, A.-M. Kitto, J. Atmos. Chem. 15 (1992) 133.
[101] R.C. Robbins, R.D. Cadle, J. Phys. Chem. 62 (1958) 469.
[102] R.D. Cadle, R.C. Robbins, Atmospheric Reactions Involving Aerosols, 1960, p. 155.
[103] H.F. Johnstone, G.C. Williams, Ind. Eng. Chem. 31 (1993) 1939.
[104] A.C. Baldwin, D.M. Golden, Science 206 (1979) 562.
[105] J.J. Huntzicker, R.A. Cary, C.-S. Ling, Environ. Sci. Technol. 14 (1980) 819.
[106] P.H. McMurry, H. Takano, G.R. Anderson, Environ. Sci. Technol. 17 (1983) 347.
[107] G.O. Rubel, J.W. Gentry, J. Aerosol Sci. 15 (1984) 661.
[108] E. Swartz, Q. Shi, P. Davidovits, J.T. Jayne, D.R. Worsnop, C.E. Kolb, J. Phys. Chem. 103 (1999) 8824.
[109] P.H. McMurry, R.I. Weber, J.J. Marti, J. Aerosol Sci. 26 (1995) S205.
[110] D.J. Coffman, D.A. Hegg, J. Geophys. Res. 100 (1995) 7147.

[111] R.J. Weber, J.J. Marti, P.H. McMurry, F.L. Eisele, D.J. Tanner, A. Jefferson, Chem. Eng. Commun. 151 (1996) 53.
[112] R.J. Weber, P.H. McMurry, L. Mauldin, D.J. Tanner, F.L. Eisele, R.D. Schillawski, D. Baumgardner, J. Geophys. Res. 103 (1998) 16.
[113] V.-M. Kerminen, A.S. Wexler, S. Potukuchi, J. Geophys. Res. 102 (1997) 3715.
[114] J.W. Erisman, A.W.M. Vermetten, W.A.H. Asman, A. Waijers-Ijpelaan, J. Slanina, Atmos. Environ. 22 (1988) 1153.
[115] W.A.H. Asman, H.A. Van Jaarsveld, Atmos. Environ. 26A (1992) 445.
[116] W.D. Scott, F.C.R. Cattell, Atmos. Environ. 13 (1978) 307.
[117] I.N. Tang, H.R. Munkelwitz, J. Aerosol Sci. 8 (1977) 321.
[118] I.N. Tang, H.R. Munkelwitz, J.G. Davis, J. Aerosol Sci. 9 (1978) 505.
[119] I.N. Tang, J. Aerosol Sci. 7 (1976) 361.
[120] I.N. Tang, W.T. Wong, H.R. Munkelwitz, Atmos. Environ. 15 (1981) 2463.
[121] P. Saxena, T.W. Peterson, J. Colloid Interf. Sci. 79 (1981) 496.
[122] J.F. Spann, C.B. Richardson, Atmos. Environ. 19 (1985) 819.
[123] A.W. Stelson, Aerosol Sci. Tech. 23 (1995) 392.
[124] I.N. Tang, H.R. Munkelwitz, J. Geophys. Res. (1995) 18801.
[125] M.-T. Nguyen, A.J. Jamka, R.A. Cazar, F.-M. Tao, J. Phys. Chem. 106 (1997) 8710.
[126] F.-M. Tao, J. Phys. Chem. 108 (1998) 193.
[127] G. Feick, J. Am. Chem. Soc. 76 (1954) 5858.
[128] G. Feick, R. Hainer, J. Am. Chem. Soc. 76 (1954) 5860.
[129] J.D. Brandner, N.M. Junk, J.W. Lawrence, J. Robins, J. Chem. Eng. Data 7 (1962) 227.
[130] A.W. Stelson, S.K. Friedlander, J.H. Seinfeld, Atmos. Environ. 13 (1979) 369.
[131] G.J. Doyle, E.C. Tuazon, R.A. Graham, T.M. Mischke, A.M. Winer, J. Pitts, N. James, Environ. Sci. Technol. (1979) 1416.
[132] B.R. Appel, S.M. Wall, Y. Tokiwa, M. Haik, Atmos. Environ. 14 (1980) 549.
[133] J. Forrest, R.L. Tamer, D. Spandau, T. D'Ottavio, L. Newman, Atmos. Environ. 14 (1980) 137.
[134] A.W. Stelson, J.H. Seinfeld, Atmos. Environ. 16 (1982) 993.
[135] A.W. Stelson, J.H. Seinfeld, Atmos. Environ. 16 (1982) 983.
[136] I.N. Tang, Atmos. Environ. 14 (1979) 819.
[137] P. Dingermans, Recl. Trav. Chim. Pay-B. 60 (1941) 317.
[138] H. Stephen, T. Stephen, in: H. Stephen, T. Stephen (Eds.), Solubilities of Inorganic and Organic Compounds, McMillan, New York, 1963, p. 217.
[139] W.J. Hamer, Y.-C. Wu, J. Phys. Chem. Ref. Data 1 (1972) 1047.
[140] V.V. Larson, G.S. Taylor, Atmos. Environ. 17 (1983) 2489.
[141] C.B. Richardson, R.L. Hightower, Atmos. Environ. 21 (1987) 971.
[142] R.A. Brost, A.C. Delany, B.J. Huebert, J. Geophys. Res. 93 (1988) 7137.
[143] R.M. Harrison, W.T. Sturges, A.-M. Kitto, Y. Li, Atmos. Environ. 24A (1990) 1883.
[144] B.J. Huebert, W.T. Luke, A.C. Delany, R.A. Brost, J. Geophys. Res. 93 (1988) 7127.
[145] A.G. Allen, R.M. Harrison, J.W. Erisman, Atmos. Environ. 23 (1989) 1591.
[146] R.M. Harrison, W.T. Sturges, A.-M. Kitto, Y. Li, Atmos. Environ. 24A (1990) 1883.
[147] G. Lammel, G. Pohlmann, J Aerosol Sci 23 (1992) S941.
[148] M. Bassett, J.H. Seinfeld, Atmos. Environ. 17 (1983) 2237.
[149] A.W. Stelson, J.H. Seinfeld, Atmos. Environ. 16 (1982) 2507.
[150] M. Bassett, J.H. Seinfeld, Atmos. Environ. 18 (1984) 1163.
[151] C.K. Chan, R.C. Flagan, J.H. Seinfeld, Atmos. Environ. 26A (1992) 1661.
[152] C. Seigneur, P. Saxena, A.B. Hudichewsky, Sci. Total Environ. 23 (1982) 283.
[153] R.L. Tanner, Atmos. Environ. 16 (1982) 2935.
[154] R.L. Hightower, C.B. Richardson, Atmos. Environ. 22 (1988) 2587.
[155] L.M. Hildemann, A.G. Russell, G.R. Cass, Atmos. Environ. 18 (1984) 1737.
[156] C.C. Stephenson, J. Chem. Phys. 12 (1944) 318.
[157] E. Clementi, J. Chem. Phys. 46 (1967) 3851.
[158] P. Goldfinger, G. Verhaegen, J. Chem. Phys. 50 (1969) 1467.
[159] S. Shibata, Acta Chem. Scand. 24 (1970) 705.
[160] C.G. de Kruif, J. Chem. Phys. 77 (1982) 6247.
[161] R.A. Cazar, A.J. Jamka, F.-M. Tao, J. Phys. Chem. 102 (1998) 5117.
[162] J.A. Snyder, R.A. Cazar, A.J. Jamka, F.-M. Tao, J. Phys. Chem. A 103 (1999) 7719.
[163] F.-M. Tao, J. Chem. Phys. 110 (1999) 11121.
[164] B. Cherng, F.-M. Tao, J. Chem. Phys. 114 (2001) 1720.
[165] S. Twomey, J. Chem. Phys. 31 (1959) 1684.
[166] M. Luria, B. Cohen, Atmos. Environ. 14 (1980) 665.
[167] R.J. Countess, J. Heicklen, J. Phys. Chem. 77 (1973) 444.
[168] C.A. Pio, R.M. Harrison, Atmos. Environ. 21 (1987) 1243.
[169] C.A. Pio, R.M. Harrison, Atmos. Environ. 21 (1987) 2711.
[170] H. Wagner, K. Newman, J. Phys. Chem. 21 (1961) 51.
[171] T.J. Edwards, G. Maurer, J. Newman, J.M. Prausnitz, Am. Inst. Chem. Eng. J. 24 (1978) 966.
[172] D. Beutier, H. Renon, Ind. Eng. Chem. Proc. DD. 17 (1978) 220.
[173] E.W.-G. Diau, T.-L. Tso, Y.-P. Lee, J. Phys. Chem. 94 (1990) 5261.
[174] F. Stuhl, J. Chem. Phys. 59 (1973) 635.
[175] R.G. de Pena, K.J. Olszyna, J. Heicklen, J. Phys. Chem. 77 (1973) 438.
[176] K.J. Olszyna, R.G. De Pena, M. Luria, J. Heicklen, Aerosol Sci. 5 (1974) 421.
[177] G.O. Rubel, J.W. Gentry, J. Phys. Chem. 88 (1984) 3142.
[178] G.O. Rubel, J.W. Gentry, Particul. Technol. 3 (1985) 37.
[179] P. Saxena, C. Seigneur, T.W. Peterson, Atmos. Environ. 17 (1983) 1315.
[180] Y.-S. Chang, G.R. Carmichael, H. Kurita, H. Ubda, Atmos. Environ. (1987) 1969.
[181] S.W. Campbell, M.C. Evans, N. Poor, Atmos. Environ. 36 (2002) 4299.
[182] G. Kramm, R. Dlugi, J. Atmos. Chem. 18 (1994) 319.
[183] A.G. Russell, G.J. McRae, G.R. Cass, Atmos. Environ. 17 (1983) 949.
[184] W.A.H. Asman, A.J. Janssen, Atmos. Environ. 21 (1987) 2099.
[185] B.E.A. Fisher, Atmos. Environ. 18 (1984) 553.
[186] M.V. Galperin, M.A. Sofiev, O.G. Afinogenova, Water Air Soil Poll. 85 (1995) 2051.
[187] M.V. Galperin, M.A. Sofiev, Atmos. Environ. 32 (1998) 373.
[188] R. Singles, M.A. Sutton, K.J. Weston, Atmos. Environ. 32 (1998) 393.
[189] H.M. ApSimon, B.M. Barker, S. Kayin, Atmos. Environ. 28 (1994) 665.
[190] F.J. Dentener, P.J. Crutzen, J. Atmos. Chem. 19 (1994) 331.
[191] M. Nielsen, S. Ott, H.E. Jorgensen, R. Bengtsson, K. Nyren, S. Winter, D. Ride, C. Jones, J. Hazard. Mater. 56 (1997) 59.
[192] D.M. Deaves, S. Gilham, B.H. Mitchell, P. Woodburn, A.M. Shepherd, J. Hazard. Mater. A88 (2001) 1.